Mine detection and classification using optical sensors

Initial results

INGMAR RENHORN, STAFFAN CRONSTRÖM, HÅKAN LARSSON, ROLAND LINDELL,
THOMAS SVENSSON, GUSTAV TOLT, NICLAS WADSTRÖMER

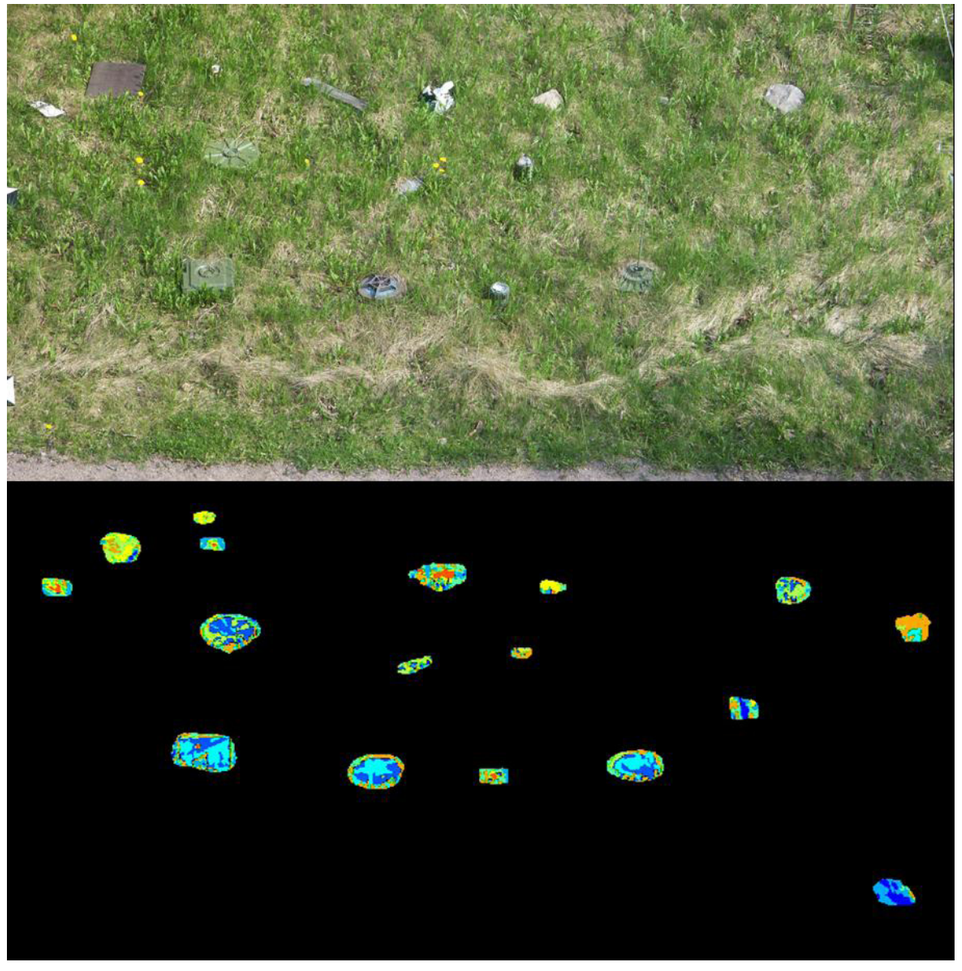

FOI, Swedish Defence Research Agency, is a mainly assignment-funded agency under the Ministry of Defence. The core activities are research, method and technology development, as well as studies conducted in the interests of Swedish defence and the safety and security of society. The organisation employs approximately 1000 personnel of whom about 800 are scientists. This makes FOI Sweden's largest research institute. FOI gives its customers access to leading-edge expertise in a large number of fields such as security policy studies, defence and security related analyses, the assessment of various types of threat, systems for control and management of crises, protection against and management of hazardous substances, IT security and the potential offered by new sensors.

FOI
Defence Research Agency
Sensor Systems
P.O. Box 1165
SE-581 11 Linköping

Phone: +46 13 37 80 00
Fax: +46 13 37 81 00

www.foi.se

FOI-R--2496--SE Scientific report
ISSN 1650-1942 March 2008

Sensor Systems

Ingmar Renhorn, Staffan Cronström, Håkan Larsson, Roland Lindell, Thomas Svensson, Gustav Tolt, Niclas Wadströmer

Mine detection and classification using optical sensors

Initial results

Titel	Detektion och klassificering av minor med elektrooptiska metoder – Inledande resultat
Title	Mine detection and classification using optical sensors -- Initial results
Rapportnr/Report no	FOI-R--2496--SE
Rapporttyp Report Type	Vetenskaplig rapport Scientific report
Sidor/Pages	45 p
Månad/Month	Mars/March
Utgivningsår/Year	2008
ISSN	ISSN 1650-1942
Kund/Customer	FM
Forskningsområde Programme area	4. Sensorer och signaturanpassning 4. Sensors and Low Observables
Delområde Subcategory	42 Sensorer 42 Sensors
Projektnr/Project no	E3084
Godkänd av/Approved by	Lena Klasén

FOI, Totalförsvarets Forskningsinstitut
Avdelningen för Sensorsystem
Box 1165
581 11 Linköping

FOI , Swedish Defence Research Agency
Sensor Systems
P.O. Box 1165
SE-581 11 Linköping

Sammanfattning

Optiska sensorsystem har med framgång utnyttjats för detektion av ytlagda minor på avsevärda avstånd i ett stort antal scenarier. Både passiva och aktiva hyperspektrala sensorer har påvisat hög kapacitet för automatisk detektion av minor och andra objekt och förmåga att visa in högupplösande sensorsystem för identifiering.

Värdering av sensorsystemkombinationer försvåras av att prestanda beror även på förmågan hos utnyttjade detektionsalgoritmer. Här införs en informationsteoretisk ansats för att erhålla algoritmoberoende jämförelser.

Tyngdpunkten i detta projekt är att ta fram nya idéer för optisk detektion, signalbehandling, mål- och bakgrundskarakterisering samt egenskapsextraktion för att erhålla förbättrad detektion och förbättrad klassningsförmåga. Det finns fortfarande viktig fenomenologi som ännu ej undersökts såsom polarimetriska egenskaper, emissivitetsvariationer i det termiska våglängdsområdet samt vilka fördelar som kan erhållas med tredimensionell avbildning.

Nyckelord:

truppminor, fordonsminor, detektion av landminor, optiska sensorsystem, signalbehandling

Summary

There are many tactical scenarios where optical sensor systems are proving promise in detecting surface-laid mines at substantial stand-off distance. Both passive and active hyperspectral sensors have shown high capability in automatically detecting mines and other man-made objects and the capability to cue other high resolution sensors for identification.

Evaluation of sensor system combinations are typically hampered by detection algorithm capability uncertainties. Information theory is being invoked in order to obtain algorithm independent comparisons of sensor suits.

The emphases of this project is to obtain new ideas for optical sensing, signal processing, target and background characterisation and data and feature fusion in order to improve on mine detection and classification performance. Important phenomenology for mine detection has still to be explored, such as polarimetric properties, emissivity variation in the long wave infrared spectral region and the benefit of detailed three dimensional imaging.

Keywords:

anti-personnel mines, antitank mines, land-mine detection, optical sensor systems, signal processing

Table of contents

1 Introduction 7

2 Remote detection issues 8

3 Sensor technologies 9

4 Phenomenology 11

4.1 Solar irradiance and atmospheric effects 11

4.1.1 Atmospheric transmission 12
4.1.2 Solar irradiance as a function of solar elevation 13

4.2 Bidirectional reflectance distribution function 15

4.2.1 BRDF models for reflective surface and diffuse surface 16

4.3 Radiometry 16

5 Spectral signatures 18

5.1 Surface land mines and occluded land mines 18

5.1.1 Reflectivity and emissivity 18

5.2 Buried land mines and disturbed soil 20

6 Signal processing considerations 21

6.1 Receiver operating characteristics 21

6.2 Mutual information 24

7 Preliminary signal processing results 27

7.1 Hyperspectral sensor in VNIR 27

7.2 Multispectral sensor in SWIR/MWIR 33

7.3 Long wave thermal infrared sensor 35

7.4 White light illumination 39

8 Discussion and conclusions 44

9 References 45

1 Introduction

No single mine detection and classification sensor has shown the performance needed in order to fulfil the requirements in an operational scenario. There are however specific tasks that can be performed and this combination of sensors and tasks could potentially be useful. Infrared and multi/hyperspectral sensors are showing promise to be used in detecting surface-laid mines at substantial stand-off distance, providing information extraction capability on several mine properties such as size, temperature, spectral and polarimetric properties. The sensors can be passive relying on thermal radiation or reflected solar radiation and active relying on an artificial source, e.g. a laser illuminator. The detection of surface mines is possible for an observer at close range but automatic systems are still of interest in wide-area search using e.g. airborne sensors. A general overview of the mine detection area has been previously reported [1].

Although large mine detection programs has been carried through, there is little information yet published on the operating characteristics (ROC) of the receivers. A reason for this is that the performance depends on not only the sensor systems but also on the type of mines and the environmental conditions. This has resulted in a great number of concept demonstrations and studies of specific phenomena such as thermal contrast as a function of weather parameters. Detection of mine fields is typically much easier than the detection of single mines. For an optical system, a large enough mine surface must be exposed to the sensor in order to render a detection. With a large number of mines, the likelihood that some mines will be exposed is increasing. They will also permit increased classification capability from geometry and spectral pattern analysis. The engagement in international operations brings about new and difficult environments including forested or mountainous terrain as well as operations in urban environments against irregular forces.

Mine detection has been demonstrated with a variety of optical sensor technologies covering the wavelength region from the ultraviolet (UV), visible and near infrared (VNIR), short wave infrared (SWIR), mid wave infrared (MWIR) to the long wave thermal infrared (LWIR). Both hyperspectral imaging (HSI) and multispectral imaging (MSI) has been demonstrated including in some cases polarisation information. Active hyperspectral imaging sensors with a pulsed artificial light source can be used in order to relax natural irradiance requirements. The artificial light source can be broadband in the VNIR spectral region. Irradiation with a monochromatic light source can be used for specific light-matter interactions such as fluorescence time decay.

The emphases of this project is to obtain new ideas for optical sensing, signal processing, target and background characterisation and data and feature fusion in order to improve on mine detection and classification performance. Both new enabling technologies and new system concepts are of interest. The purpose of signal processing is to extract reliable target detection information from sensor data with a low false alarm rate and also be able to form target models and build feature databases for classification and recognition.

2 Remote detection issues

This research program is focusing on remote detection of surface laid mines and minefields at a standoff distance. Neutralization techniques will not be treated here. Data from collection sensor platforms, initially static ones, are being used for algorithm development and phenomenology assessment. A number of optical sensor technologies are being investigated such as staring focal plane arrays, multi/hyperspectral, passive polarisation, active illumination and 3-D LADAR sensors. Mine signatures related to these sensing technologies are catalogued in order to support evaluation of mine detection algorithms. As a result of the evaluation process, a down-selection of sensor technologies for specific platform sensor suits will be carried through.

Thermal detection of both surface laid mines and buried mines attempt to take advantage of the difference in thermal conductivity and specific heat, i.e. the difference in heating and cooling rate between the mine or the disturbed soil above the mine and the surrounding soil. The thermal contrast will depend on the solar loading, ambient air temperature, soil moisture and emissivity. Modelling of the optimal circumstances for detection has not yet been determined.

The optimal multi-sensor suit with respect to sensor fusion and automatic target recognition in order to improve detection performance while reducing the number of false alarms will be established using e.g. information theory. Based on preliminary results, a first integration for sensor fusion/ATR will be suggested. More sensors will be added as supporting results are being obtained and new optimizations of the multi-sensor fusion approaches will be evaluated.

Two main scene geometries with standoff detection capability, down-looking and forward-looking, are being investigated. In order to support the methodology for evaluation of detection algorithms, mine signature simulations related to the signature database is developed. The optimal sensor combination is likely to be different in the two cases, since the phenomenology and appearance will be different.

Assessment of ROC of the sensor system using a small number of targets (mines) and interfering objects (clutter) with restricted variability is a challenge. Several steps are being evaluated. In a first step, each mine and clutter object is treated individually in order to understand the interfering mechanism. In a second step, these results are combined with an estimate of the likelihood of observing a mine in the specific state. The state of appearance and the degree of clutter will depend on the characteristics of the terrain. A measured variation in mine appearance is therefore required for each type of terrain.

The operational speed can to some degree be varied depending on e.g. cost, size, weight, and maturity or risk considerations. In the final end, brass board detection systems should be realized for improved probability of detection and reduced false alarm rates while increasing operational speeds.

3 Sensor technologies

Extensive experiments have been conducted using a large number of sensors [2]. Even so, some domains of variability have not been explored both from a phenomenology point of view and from a scene variability point of view including seasonal variations. There are several phenomena that have not yet been explored. The sensor equipments being used in the field trials are shown in the tables I and II. Missing domains are also indicated and serious shortcomings noted (0).

Table I. Passive optical sensors. SC – Single spectral channel, MS – Multispectral, HS – Hyperspectral, P – Polarimetric, X – Tested in field trial, x – Tested in laboratory, 0 – Still to be tested.

Spectral region	SC	MS	HS	P
VNIR		X	X	
SWIR		X	X	
MWIR		X		0
LWIR	X	0	0	0

Polarimetric imaging in the MWIR and LWIR has been shown to contribute to the characteristics of mine surfaces. There is however still a need to find out to what extent this information is adding critical information with respect to other characteristics.

Table II. Active optical sensors. 3-D – laser radar, Illumination – active illumination, P – Polarimetric, X – Tested in field trial, x – Tested in laboratory, 0 – Still to be tested.

Spectral region	3-D	Illumination	P
VNIR		X	0
SWIR	X	X	x
MWIR			
LWIR			

Hyperspectral sensors collect data in many contiguous spectral bands, often of the order of several hundred. Spectral information improves on the discrimination capability with respect to background clutter and also supports signature based detection and classification. Signal processing in real time enhances the operational capability of these systems. Dedicated parallel processing is needed in order to reduce the delay in making the information available.

Multispectral sensor systems could potentially produce useful capabilities by careful selection of the spectral bands with respect to both target and clutter characteristics. The advantage with multispectral systems stems from larger coverage capability and also the possibility to incorporate micro-polarisers directly on the focal plane array. In the long wave thermal infrared spectral region, filters could be selected to emphasize variations in emissivity together with the polarimetric characteristics. This has applications in e.g. disturbed soil detection.

Hyperspectral sensor systems have proven very effective in automatic target detection, especially in the visible and near infrared spectral region. For night operations, illumination is needed with a broad band source. The performance of such systems compares quite favourably with the daylight systems due to reduced shadowing effects but they do have substantially increased power requirements.

There is a fundamental difference in polarisation exploitation of passive sensor data compared to active sensor data. Passive polarimetric imagery is of greatest interest in the thermal infrared and for object surfaces being monitored close to Brewster angle. For this angle, the degree of polarisation will be larger than for natural background. In active

imagery, the depolarisation of the polarised illumination of the scene is being studied. There will be a difference in depolarisation depending on the ratio between surface scattering and bulk multiple scattering. This can be exploited for target/background contrast enhancement.

High spatial resolution data, both two-dimensional and three-dimensional, can be used for target recognition. In order to reduce the amount of data that has to be processed, multi- and/or hyperspectral sensors are used for cuing.

The detection approach depends on how the mines are being deployed. Detection of e.g. buried antipersonnel mines (APM) is one of the greater challenges. They are made of non-metallic materials and much smaller than the antitank mines. There are different types of APMs with variations in the killing mechanism. Blasting mines are usually buried underground but some are scattered from airplanes or dispersed in rivers. Bounding fragmentation mines are larger and can be buried or placed on surface. When activated, they bounce up and detonate causing harm at a greater distance. Directional fragmentation mines are mostly deployed on the surface. The lethal range can be over 200 m.

Different types of mines will most likely require different types of feature extraction for detection and classification. It is therefore of interest to come up with a mine taxonomy that serves the purpose of both indicating the type of mine and the possible features available for detection.

4 Phenomenology

The climate change problem has resulted in increased research in the solar irradiance budget components. Much information on a global scale has been obtained from satellite observations. Models has been developed that accounts for both direct and diffuse spectral components in the 0.2-4.0 μm region. For anomaly detection, shadowing effects pose a serious problem. Diffuse illumination due to clouds can be beneficial for the sensor performance due to the lower scene contrast. System availability is limited by the amount of daylight, which varies with latitude and time of the year. Active illumination is resulting in very little shadowing but puts high demands on illumination uniformity and irradiance levels.

Multispectral- and hyperspectral imaging has proven powerful in anomaly detection of objects in a cluttered background. Active illumination has been shown to produce viable results. Combining illumination with controlled polarisation properties with a polarimetric sensor has the potential to enhance the target/background contrast and improve on detection probabilities of low contrast targets. The coherence property of the illuminator is still a subject of concern. Illuminating the scene with a coherent source can lead to substantial decrease of the image quality due to speckle noise.

The spectral properties of mines and potential clutter in the thermal infrared region have not been studied well enough in order to be evaluated. Using hyperspectral sensors in this spectral region permits the separation of temperature and emissivity. The emissivity of man made objects and clutter varies slowly with wavelength in this spectral region and could potentially be used for mine detection with day/night capability. Especially vegetation has a spectral signature that deviate from e.g. painted surfaces. The influence from the atmosphere, especially due to the variability in water vapour content, can be considerable. It has been shown however, that this influence can be taken care of using scene data and detailed atmospheric models [3]. These phenomena should be further studied in order to evaluate the potential night capability.

The performance of thermal imagers is sometimes limited by the small thermal contrast between target and background. In polarimetric imaging, the difference in polarisation of the emitted radiation between the target and the background is detected. Polarimetric data depends on the target surface properties and its orientation and depends minimally on the temperature [4]. Natural background such as grass, sand or gravel emits and reflects radiation that is less polarised.

4.1 Solar irradiance and atmospheric effects

The illumination of the ground depends on the solar zenith angle. The solar zenith angle is the angle from the zenith to the solar position in the sky. The zenith angle depends on latitude, solar declination angle and time of day. The solar declination angle depends on the time of the year. The zenith angle is given by

$$\theta = \cos^{-1}\left(\sin\Phi\sin\delta + \cos\Phi\cos\delta\cos H\right) \tag{1}$$

where Φ is the latitude, δ is the solar declination angle and H is the angle of radiation due to the time of day. Time is given in solar time as the hour of the day from midnight. The parameter H is given by

$$H = \frac{15\pi}{180}\left(Time - 12\right) \text{ [rad]} \tag{2}$$

The solar declination angles for the northern hemisphere is derived from the following fix points:

- Vernal Equinox Mar. 21/22 δ=0°
- Summer Solstice Jun. 21/22 δ=23.5°
- Autumnal Equinox Sept. 21/22 δ=0°
- Winter Solstice Dec. 21/22 δ=-23.5°

The solar declination angle can be approximated by

$$\delta = -\frac{23.5\pi}{180}\cos\left(\frac{day+10}{365}\frac{\pi}{180}\right) \text{ [rad]} \quad (3)$$

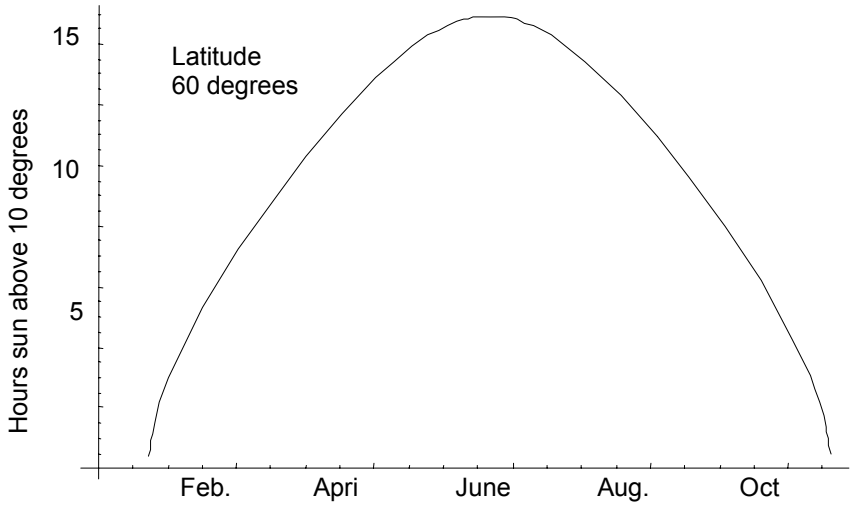

Fig. 1. The availability of optical systems relying on reflected solar radiation increases as shown towards midsummer for a latitude of 60 degrees. The sun is always below 10 degrees elevation during almost three winter months.

4.1.1 Atmospheric transmission

The atmosphere alters the spectral irradiance at earth's surface significantly. The spectral transmission, $\tau_{down}(\lambda)$, is governed by both molecular absorption and aerosol scattering. A typical transmission spectrum is shown in figure 2 for the elevation angles 30 and 60 degrees. The absorption bands of water vapour and carbon dioxide are pronounced. The decrease in transmittance in the short wavelength spectral region is due to *Rayleigh scattering* from air molecules with a λ^{-4} dependence on wavelength. With aerosols present, *Mie scattering* is also affecting the transmission. For large particles, this scattering is wavelength independent. For particle sizes in the range λ/π and $2\lambda/\pi$, there is a wavelength dependence that is less than that of Rayleigh scattering. Attenuation in a real atmosphere is of course due to a combination of molecular absorption, Mie and Rayleigh scattering and particle absorption.

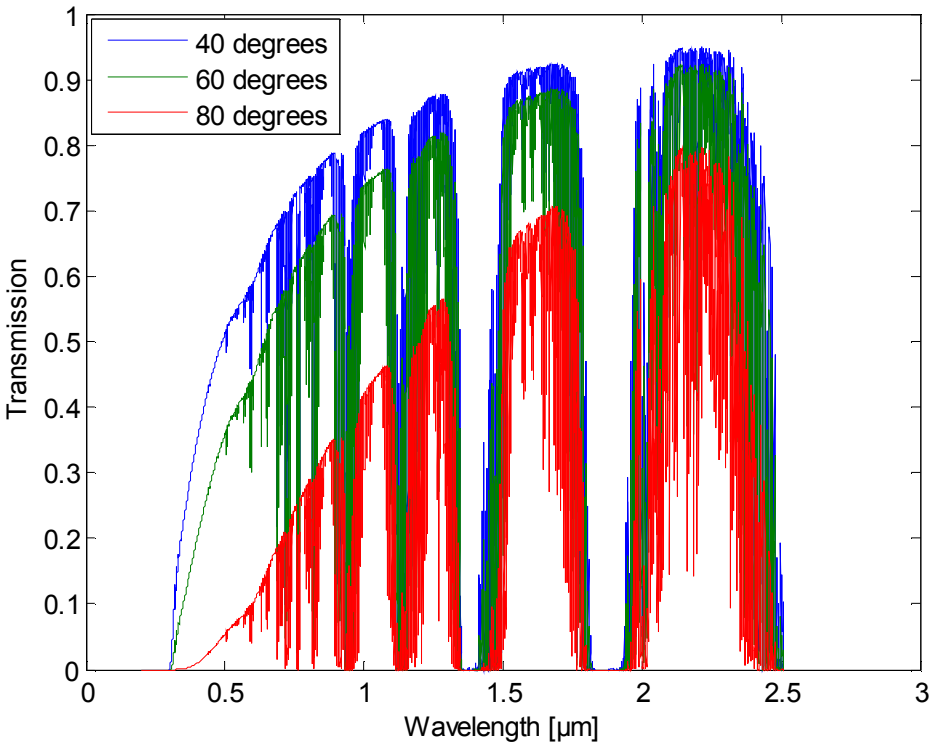

Fig. 2. Transmittance of the atmosphere as calculated by the code MODTRAN. The solar elevation angles are between 10 and 50 degrees or zenith angles between 40 and 80 degrees. The absorption bands are primarily due to water vapour and carbon dioxide. The atmospheric model is “subarctic summer” and a “visibility” of 23 km is assumed.

4.1.2 Solar irradiance as a function of solar elevation

The solar irradiance is given by

$$E_{sun}(\lambda) = \tau_{down}(\lambda) L_{sun}(\lambda) d\Omega_{sun} Cos(\theta)$$

$$E_{sun}(\lambda) = \tau_{down}(\lambda) E^{0}_{sun}(\lambda) Cos(\theta) \qquad (4/5)$$

where $\tau_{down}(\lambda)$ is the solar path atmospheric transmittance and θ is the angle between the surface normal and the direction of incidence of the irradiance. The atmospheric transmission depends on the solar elevation. The spectral solar irradiance at ground level is illustrated in figure 3 for three elevation angles, 10, 30 and 50 degrees respectively.

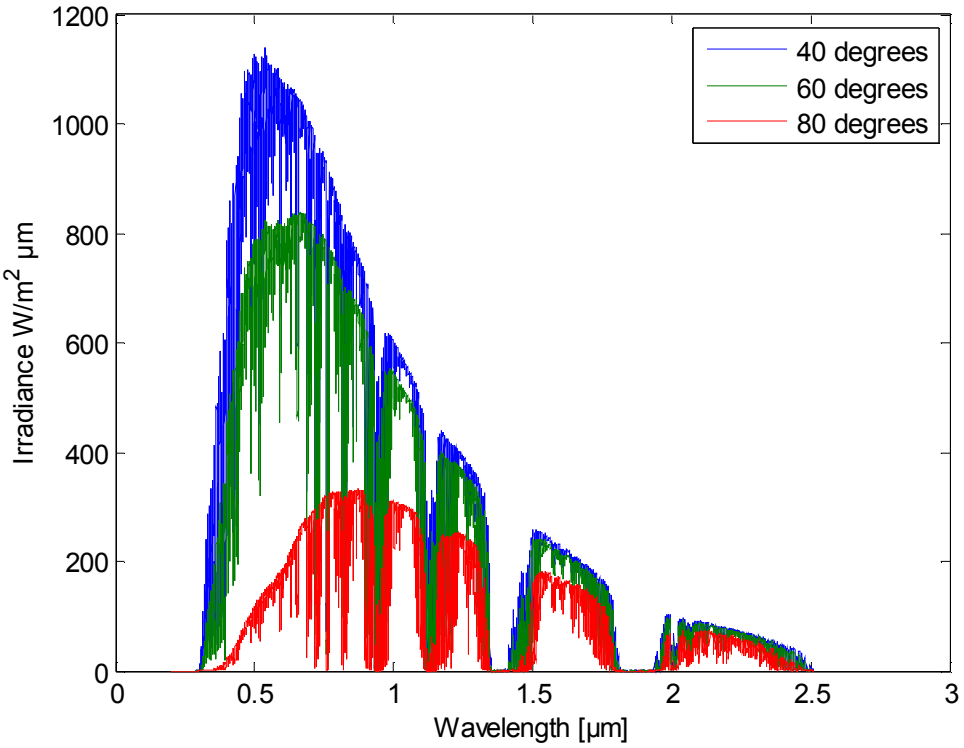

a)

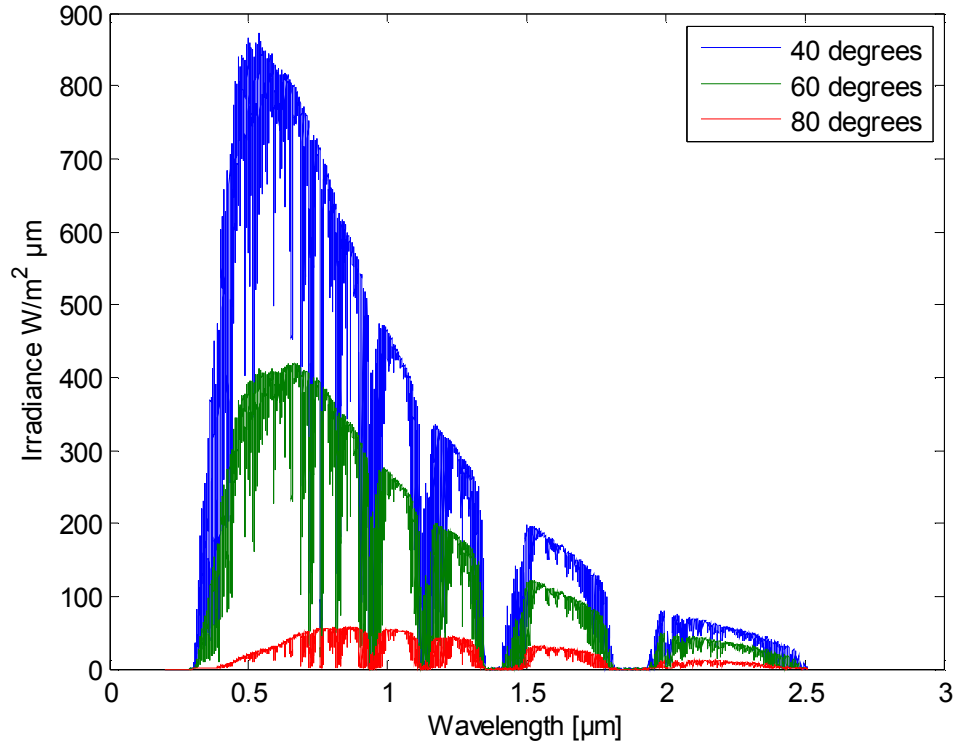

b)

Fig. 3. Solar irradiance in the visible, near infrared and short wave infrared at ground level for elevation angles between 10, 30 and 50 degrees or zenith angles 40, 60 and 80 degrees where figure a) is for a surface perpendicular to the irradiance and b) is for a surface with normal in nadir direction.

4.2 Bidirectional reflectance distribution function

The surface characteristics of painted objects such as mines and mine-like objects deviate substantially from natural background. The deferens can be observed both with respect to spectral properties, surface scattering properties and with respect to effects on the state of polarisation. It is therefore important to characterise surfaces of interest and build a relevant material database. The *bidirectional reflectance distribution function* (BRDF) is a 4-dimensional function that defines how radiation is reflected at a surface and is used to characterize the surfaces.

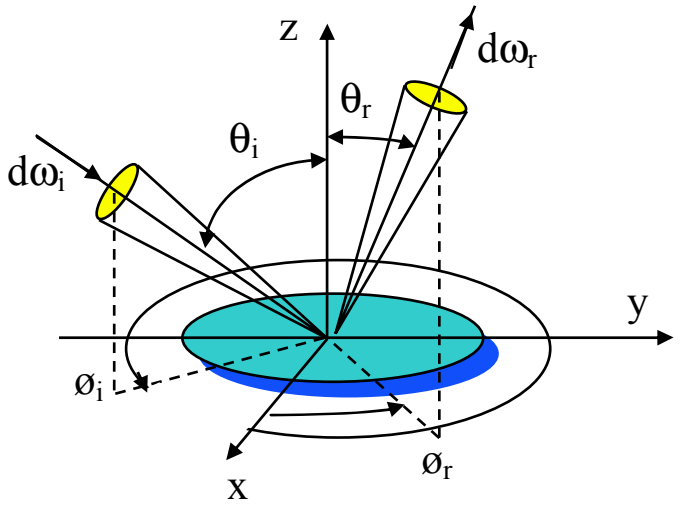

Fig. 4. Definition of angles in connection to BRDF measurements.

When determining the scattering properties of a surface, an area large compared to the wavelength but still small enough to be considered to be homogeneous must be selected. Illumination is within a solid angle Ω_i that can be small for collimated illumination or cover the whole hemisphere 2π sr. The zenith angle is denoted θ_i and the azimuth angle is denoted ϕ_i. For an isotropic material, the scattering properties depend only on the difference in the azimuth between incoming and reflected radiation. Therefore, the centre of the irradiance azimuth, ϕ_{io} , is conveniently set to $-\pi$ rad.

The irradiance E at the surface is given by

$$E = \int_0^{2\pi} \int_0^{\frac{\pi}{2}} L_i(\theta,\phi)\cos(\theta)\sin(\theta)\,d\theta\,d\phi \ , \tag{6}$$

where $L_i(\theta, \phi)$ describes the angular variation of the incident radiation. BRDF is defined by the relation

$$L_r(\theta_r,\phi_r) = \int_0^{2\pi} \int_0^{\frac{\pi}{2}} \rho(\theta_i,\phi_i,\theta_r,\phi_r) L_i(\theta_i,\phi_i)\cos(\theta_i)\sin(\theta_i)\,d\theta_i\,d\phi_i \ , \tag{7}$$

where $\rho(\theta_i,\phi_i,\theta_r,\phi_r)$ depends on both the angle of incidence and the angle of reflection. This interdependency can be very complex and does not always have an analytical solution. Emissivity is given by Kirchhoff's law

$$\varepsilon(\theta_r,\phi_r) = 1 - \int_0^{2\pi} \int_0^{\frac{\pi}{2}} \rho(\theta_i,\phi_i,\theta_r,\phi_r)\cos(\theta_i)\sin(\theta_i)\,d\theta_i\,d\phi_i \ . \tag{8}$$

In accordance to the Helmholtz reciprocity theorem, we have

$$\rho(\theta_i,\phi_i,\theta_r,\phi_r) = \rho(\theta_r,\phi_r,\theta_i,\phi_i). \quad (9)$$

4.2.1 BRDF models for reflective surface and diffuse surface

In the thermal infrared spectral region, scattering from painted and metallic objects is mainly from the surface. In the visual spectral region substantial part of the scattering can be attributed to the bulk material. It is therefore natural to specifically consider two extreme surfaces, i.e. the perfectly reflecting surface (mirror) and the perfectly diffuse surface (Lambertian).

For a perfectly reflecting surface the following relation is valid

$$\rho_{MIRROR}(\theta_i,\phi_i,\theta_r,\phi_r) = \rho_M(\theta_i)\frac{\delta(\theta_r-\theta_i)\delta(\phi_r-\phi_i-\pi)}{\cos(\theta_r)\sin(\theta_r)} \ [\mathrm{sr}^{-1}] \ , \quad (10)$$

where $\rho_M(\theta_i)$ can be polarisation dependent.

For a perfectly diffuse surface, the angular dependence of the BRDF is given by

$$\rho_{DIFFUSE} = \rho_D \frac{1}{\pi} \ [\mathrm{sr}^{-1}]. \quad (11)$$

4.3 Radiometry

The spectral regions used for reconnaissance and surveillance are dictated by the atmospheric "windows" where the atmosphere is transparent. Between these "windows", gas molecules are absorbing the radiation, primarily due to water vapour and carbon dioxide. In the visible and near infrared spectral region, the radiation is dominated by reflected solar radiation, while in the thermal infrared spectral region, the radiation is dominated by the thermal radiation from the object itself. The spectral regions are summarized in table III.

Table III. Primary spectral regions used in optical sensing. Small variations in the values of spectral boundaries can be found in different references.

Name	Wavelength range	Radiation source	Surface property of interest
Visible (V)	0.4-0.7 µm	Solar	Reflectance
Near InfraRed (NIR)	0.7-1.1 µm	Solar	Reflectance
Short Wave InfraRed (SWIR)	1.1-2.5 µm	Solar	Reflectance
Mid Wave InfraRed (MWIR)	3-5 µm	Solar Thermal	Reflectance Emissivity Temperature
Long Wave InfraRed (LWIR)	8-14 µm	Thermal	Emissivity Temperature

Spectral regions are sometimes further divided due to the finer details of the atmospheric transmission properties. E.g. the SWIR region is subdivided into 1.1-1.35, 1.4-1.8 and 2-2.5 µm regions. The MWIR 3-5 µm region is sometimes subdivided into 3-4 and 4.5-5 µm regions and the LWIR region is divided into 8-9.5 and 10-14 µm regions.

Passive sensors in the VNIR and SWIR spectral region rely on solar illumination and are therefore daylight sensors. The spectral signatures of targets and background in these

solar-reflective spectral regions are therefore defined by the reflectance as a function of wavelength. In the thermal spectral regions, the spectral signature is defined by the wavelength dependent emissivity.

The spectral radiance at the sensor is given by three main contributions. The most important contributions are the reflected downwelling irradiance at the object surface and the surface emitted radiance. Important contributions to the radiation level originate from radiation scattered by the atmosphere and from emitted upwelling radiance.

$$L_{sensor}(\lambda) = \tau_{atm}(\lambda)\varepsilon(\lambda)L_{bb}(\lambda,T) + \tau_{atm}(\lambda)\rho(\lambda)E_{sun}(\lambda) + L_{up}(\lambda) \tag{12}$$

where the spectral radiance of a blackbody source L_{bb} is given by

$$L_{bb}(\lambda,T) = \frac{2hc^2}{\lambda^5\left(e^{\frac{hc}{k\lambda T}} - 1\right)} \quad [\text{W m}^{-2}\ \text{sr}^{-1}\ \text{m}^{-1}]\ , \tag{13}$$

and where it is assumed that the relation

$$\rho(\lambda) = (1 - \varepsilon(\lambda)) \tag{14}$$

is true.

h	=	Planck´s constant
c	=	Speed of light
k	=	Boltzmann´s constant
$L(\lambda)$	=	Spectral radiance
L_{bb}	=	Blackbody radiation
L_{down}	=	Solar, sky and atmospheric downwelling radiance
L_{up}	=	Scattered solar and atmospheric upwelling radiance
$\varepsilon(\lambda)$	=	Emissivity
$\rho(\lambda)$	=	Bidirectional reflection distribution function

The various components can be calculated using the radiative transfer code MODTRAN.

5 Spectral signatures

5.1 Surface land mines and occluded land mines

Surface mines can be detected at some stand-off range. Both surface scattering properties and thermal behaviour is often quite different from the surrounding. Solar heated mines therefore often exhibit high contrast to the background. Knowledge of the sun elevation and the impact of weather conditions should be used in predicting sensor performance. The shape of the mine can also support in the classification process. This contrast is not affected by e.g. camouflage paint in the VNIR spectral region.

The spectral property of mines is often quite distinct compared to soil and vegetation. Hyperspectral detection is therefore a powerful tool for mine discrimination. If the mine is spatially resolved, a small region exhibiting a spectral anomaly is observed. The polarimetric properties can also be exploited at relatively low observation angles since material like grass in contrast to flat surfaces tend to have random polarisation. Unfortunately, mines can be obscured by vegetation at those angles.

Active illumination is of interest when solar illumination is insufficient. The polarimetric issues are here quite different from the passive situation since the illumination is polarised and flat surfaces observed even at nadir will not depolarise the radiation, while grass tend to depolarise the radiation.

5.1.1 Reflectivity and emissivity

An example of reflectance spectra of both natural background (grass) and man-made surfaces (green paint) is shown in figure 5. Even if the paint can appear quite similar to the background to the eye, the detailed reflectance spectra can deviate quite substantially. In this example, increased reflectance in the near infrared is introduced in order to simulate the decreasing chlorophyll absorption in this spectral region. Mines routinely do not exhibit this feature and will therefore show increased contrast in this spectral region.

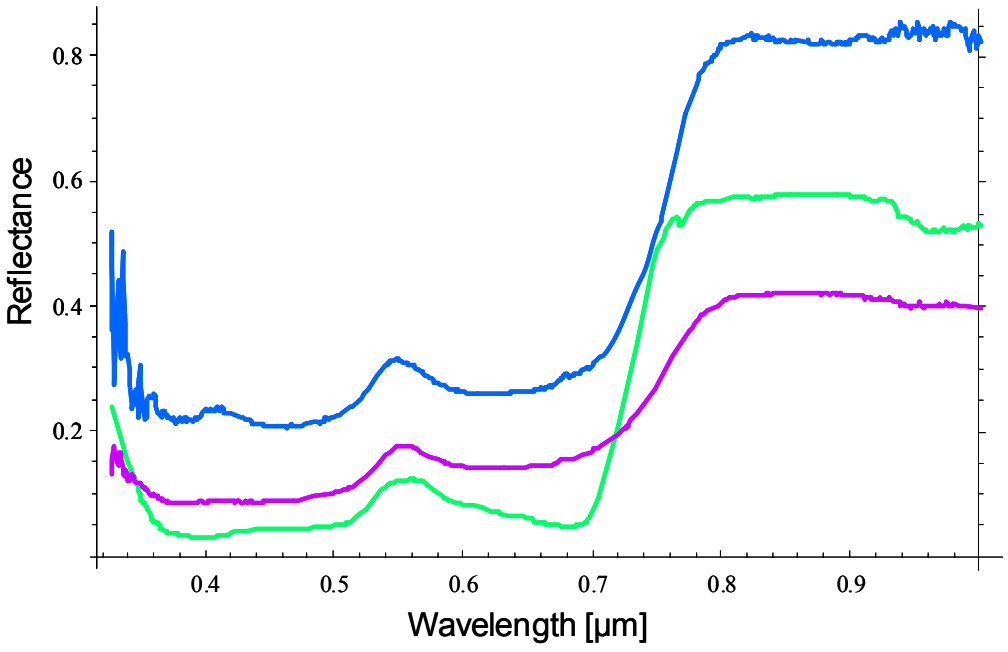

Fig. 5. Reflectance spectrum of grass (green), light green paint (blue) and dark green paint (purple).

More spectral features of the spectral radiance from objects in the visible and near infrared region is added due to atmospheric filtering. Examples of this filtering effect are shown in figure 6.

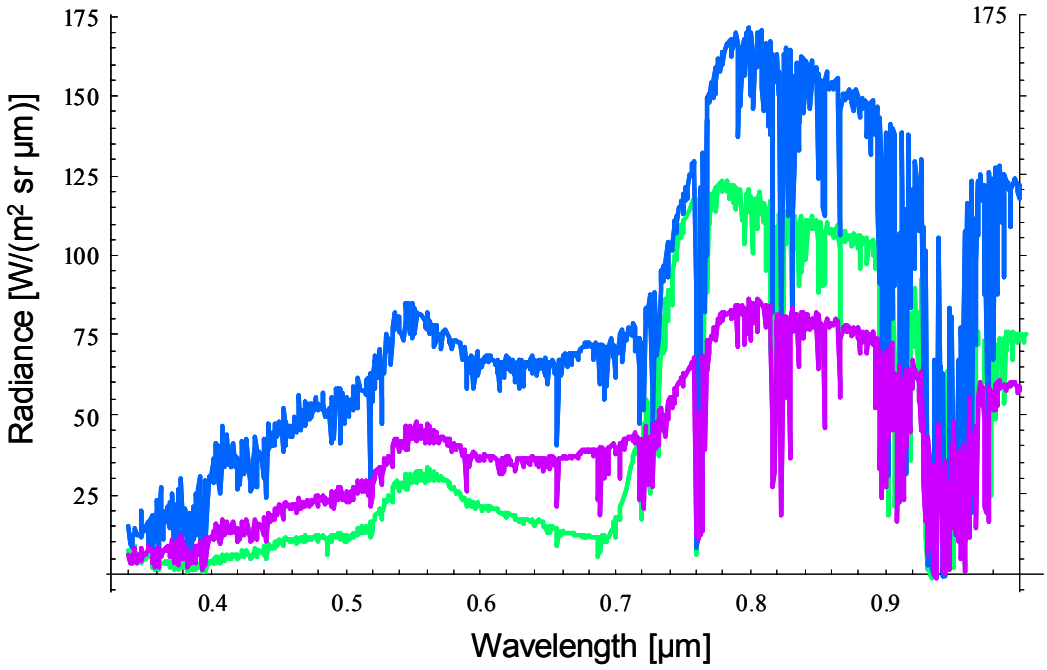

Fig. 6. Spectral radiance from grass (green), light green paint (blue) and dark green paint (purple) illuminated by sun at a zenith angle of 40 degrees.

When the spectral responsivity of the imaging hyperspectral instrument is added, the result of figure 7 is obtained.

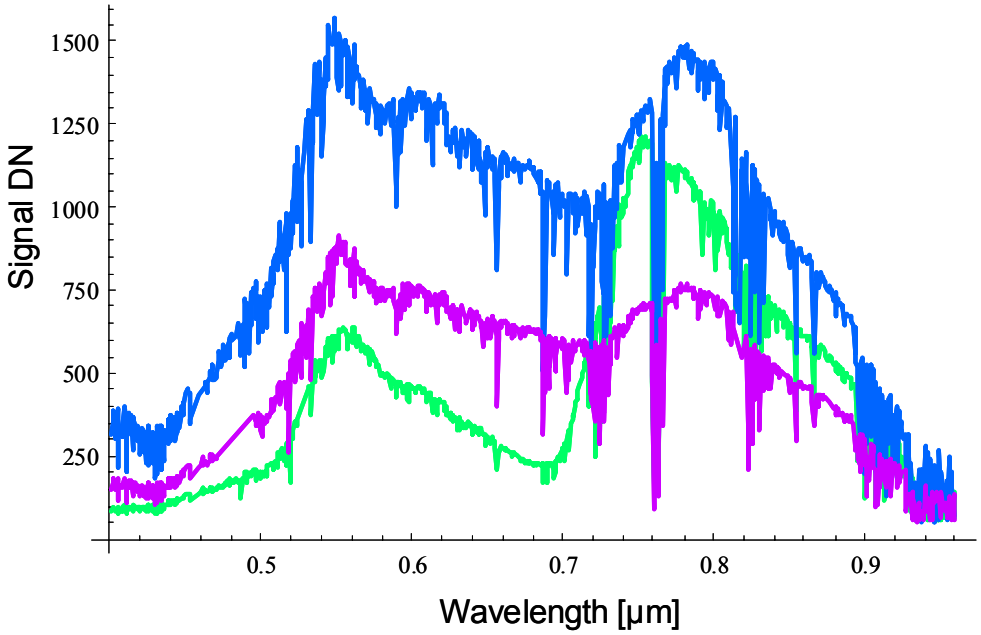

Fig. 7. Calculated signal from grass background (green), light green target (blue) and dark green target (purple) illuminated at a solar zenith angle of 40 degrees.

5.2 Buried land mines and disturbed soil

Buried antipersonnel mines are especially challenging. Thermal detection using passive sensors relies on the heating of the soil by the solar irradiance. The increase in surface temperature depends on the detailed properties of the soil such as density, moisture content, surface roughness, wind etc. These properties can be changed if the soil is disturbed by e.g. a buried mine. The diurnal solar heating and cooling tends to affect the disturbed soil differently compared to the surrounding soil. Since the mine is a better thermal insulator than the soil, this will create a measurable temperature difference that can be detected. During daytime solar load the thin layer of soil on top of the mine tends to be at higher temperature than the surrounding soil due to the fact that the mine is impeding the transport of energy to lower levels compared to the neighbouring soil. Conversely, the thin layer of soil over the mine tends to cool off more rapidly than the surrounding soil in the evening. In between these events, there will be a moment when the temperature above the mine and the surrounding will have the same temperature. If the top surface is not disturbed and the emissivity changed, the mine can not be detected at those moments. Since the temperature of the disturbed soil has a different time dependency than the homogeneous soil, time sequences can improve on the detection probability. Selecting the right time and the right weather conditions for monitoring an area is therefore crucial for thermal detection of buried mines. This is called dynamic thermography. Multispectral thermal imaging can improve on the performance with respect to temperature/emissivity separation (TES) preventing drop-out at no temperature contrast. Polarisation effects in the disturbed surface compared to the surrounding might also improve the detection capability.

The mine tends also to prevent the water to drain away during rain and to dry out more efficiently otherwise. This is causing a change in the surface particle composition of the surface and increased stress on the vegetation. This can be clearly visible and detected using e.g. hyperspectral sensors, possibly in combination with a polarimetric sensor. Under unfavourable illumination, active polarimetric systems can be used for increased contrast at close range.

6 Signal processing considerations

In this chapter we will consider a target discrimination system (figure 8) which measures target and background features. Spatial properties are not considered here. The target position is unknown. Statistical expectations may however be known or assumed and thus the occurrence is described by the stochastic variable $X \in \{b,t\}$ (b for background and t for target) with probability distribution $p_X(x)$.

The exact properties of the scene where measurement is taken place is not known but the statistical properties may be known or assumed and is described by the stochastic variable Z with conditional probability distribution $p_{Z|X}(z \mid x)$. The radiation from the scene including the targets is represented by the stochastic variable Z.

The sensor system has both random and deterministic properties and is described by the stochastic variable Y with the conditional probability distribution $p_{Y|Z}(y \mid z)$.

The detection algorithm is a deterministic function denoted $g(y)$ whose goal is to make a decision based on the sensor system output on whether a target is present or not with as low error probability as possible. We will consider the relation between the sensor system output represented by the stochastic variable Y and the occurrence of a target represented by the stochastic variable X.

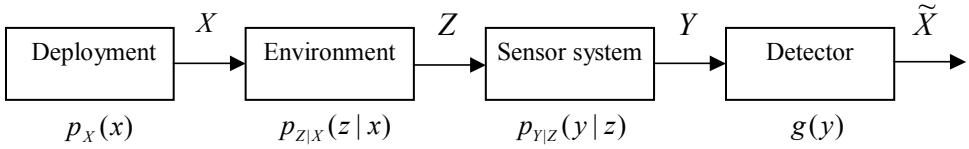

Fig. 8. A model of a target discrimination system from a signal processing point of view.

In this chapter we will only consider the relation between the sensor system output and the occurrence of a target, thus we will only consider the conditional probability distribution

$$p_{Y|X}(y \mid x) = p_{Y|Z}(y \mid z)p_{Z|X}(z \mid x) . \tag{15}$$

6.1 Receiver operating characteristics

Suppose that a signal or some feature measure, represented by the stochastic variable $X \in \Re$ with probability distribution $p_X(x)$, has to be detected in a clutter background. The signal distribution depends on whether the target is present or not. When the target is present, the signal mean will be μ_1 and when the target is absent, the mean will be μ_0. Assume for the moment that the probability distributions are normal with different means but the same variance, i.e. $p(x|\omega_i) \sim N(\mu_i, \sigma^2)$.

The detector will apply a detection threshold, x_{th}, in order to determine if the target is present or not. How well the target can be discriminated depends on the separation between the two distributions and the size of the variance. By varying the threshold, detection probabilities can be studied as a function of false alarm rates. In the same time, some targets will be missed and some clutter will be correctly rejected. The following probabilities could be considered:

$P(x > x_{th} \mid x \in \omega_1)$: detection probability with target present
$P(x > x_{th} \mid x \in \omega_0)$: false alarm probability with target absent
$P(x < x_{th} \mid x \in \omega_1)$: missing probability with target present
$P(x < x_{th} \mid x \in \omega_0)$: correct rejection probability with target absent

where

$$P(X > x_{th} \mid X \in \omega_1) = \int_{x_{th}}^{\infty} p(x \mid \omega_1) dx \tag{16}$$

and $p(x|\omega_0)$ is the corresponding probability density. This is illustrated in figure 9.

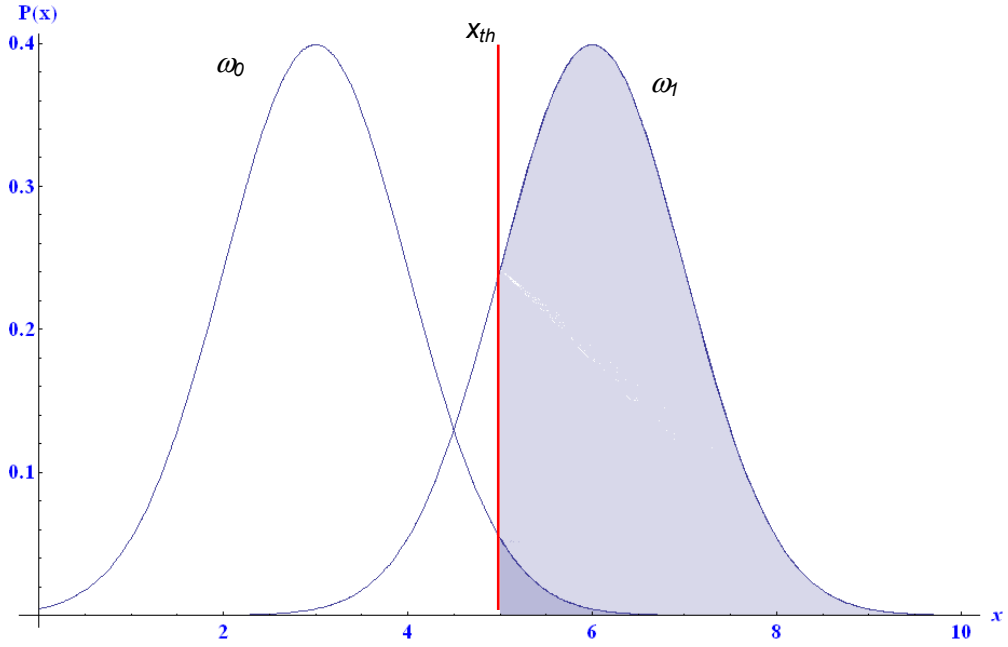

Fig. 9. Probability distribution for a normal distributed signal without and with the target present. The blue shaded area represents the area above threshold.

These probability distributions can be determined from experiments. If the probability distribution is stationary, the detection probability can be determined as a function of the change in false alarm rate. Plotting the detection probability as a function of false alarm rate is called a receiver operating characteristic (ROC) curve, see figure 10.

The ROC curve allows the study of discrimination capability as a function of decision bias. This is very useful since the target can be better characterized than background clutter. The variability in background clutter brings with it variability in false alarm rate. In order to obtain a constant false alarm rate (CFAR), which is highly desirable, the threshold has to be adaptable.

In the present applications, the feature measure X is a vector which assumes only discrete values $\{v_1,\ldots,v_m\}$. The values do not belong to an ordered set and hence the decision threshold is replaced by a decision set v_{th} which consists of all vectors considered to originate from a measurement on a target. The corresponding probability is now calculated by the corresponding sum, e.g.

$$P(X \in v_{th} \mid X \in \omega_1) = \sum_{x \in v_{th}} p(x \mid \omega_1). \tag{17}$$

where $P_D = P(X \in v_{th} \mid X \in \omega_1)$ now is the fraction of the specific target being detected. The probability to detect a number of different targets has to be further elaborated since the nature of features, ω_1, will vary with the type of target. At present, the different targets are mainly treated individually. Similar targets might be possible to order into classes where each class will have a unique set-up of features.

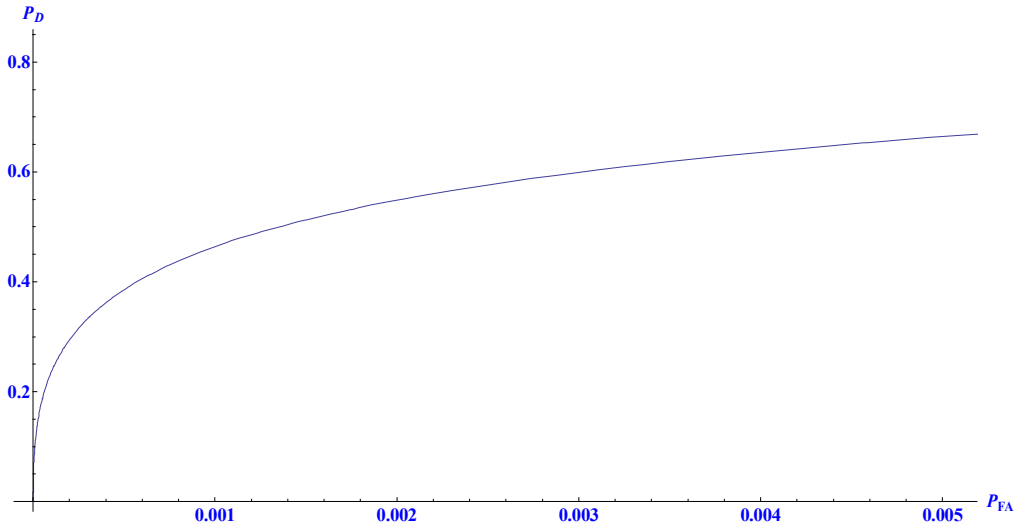

Fig. 10. Receiver operating characteristic curve (ROC). The parameter P_D is the target detection probability given by $P_D = P(X > x_{th} \mid X \in \omega_1)$. The false alarm rate (FAR) probability is given by $P_{FA} = P(X > x_{th} \mid X \in \omega_0)$.

The features present in the scene, targets and background, defines the feature total space $\omega_{scene}=\{v_1,\ldots,v_m\}$. The target feature space consists of a small part of this feature space, or $\omega_{target}=\{v_1,\ldots,v_l\}$. Assuming that targets are rare, the background feature space will be close to the total scene feature space but might deviate by some unique target features or $\omega_{background}=\{v_k,\ldots,v_m\}$. Compared to the scene feature space, the following grouping applies:

$$\omega_{scene}=\{v_1,\ldots,v_k,\ \ldots,\ v_l\ ,\ldots,\ v_m\ \}$$
$$\omega_{background}=\{\ v_k,\ \ldots,\ v_l\ ,\ldots,\ v_m\ \}$$
$$\omega_{target}=\{v_1,\ldots,v_k,\ \ldots,\ v_l\ \}$$

where the feature space $\{\ v_k,\ \ldots,\ v_l\ \}$ will be common to both the background and the target and constitutes a region where false alarms are present. The feature space $\{v_1,\ldots,v_{k-1}\ \}$ constitutes a region where the target can be detected without any false alarms.

The statistical distribution does not have to be a normal distribution as in the continuous example given above but could have any distribution. In order to build an optimal ROC curve from a general distribution, the features should be sorted in descending order with respect to $p(x \mid \omega_1) / p(x \mid \omega_0)$. If the new reordered feature space is given by $\omega_{target}=\{u_1,\ldots,u_k,\ \ldots,\ u_l\ \}$, the detection probability is obtained by summing partial detection probabilities as a function of the corresponding summed false alarm probabilities, i.e.

$$P_D = \sum_{k=1_h}^{l} p(\mu_k \mid \omega_1)$$
$$P_{FA} = \sum_{k=1}^{l} p(\mu_k \mid \omega_0) \qquad (18/19)$$

This is illustrated in figure 11.

The false alarm rate is here scaled to a probability per pixel where the scene constitutes the total number of pixels. The scene will cover a specific area why the false alarm rate also can be interpreted as a false alarm rate per unit area. This is of interest when using this information for estimating sensor performance.

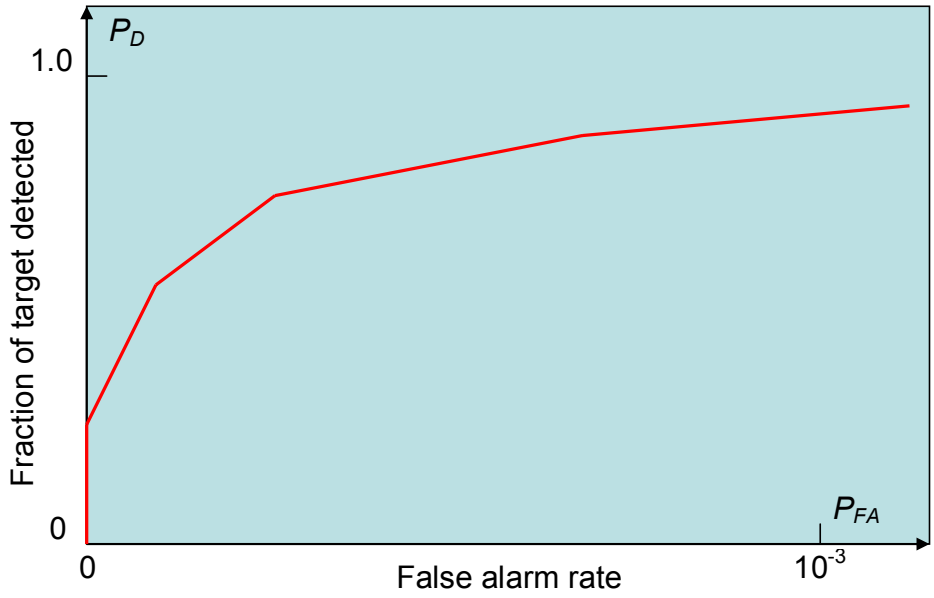

Fig. 11. ROC curve for a target in background clutter.

In a multidimensional feature space where the detection probability depends on a specific detection algorithm, it is not possible to know if the optimal ROC is approached. In practise improvements in operating characteristics is studied by varying feature approaches and varying the threshold. It is therefore desirable to find algorithm independent approaches.

6.2 Mutual information

The problem of optimizing multi-sensor performance and the difficulty to define metrics for performance assessments from the characteristics of detection algorithms has motivated the development of processing techniques based on information theory [5]. Information theory can, besides estimation of optimal detection performance, also be used for classification and identification feature extraction and for data registration. For an objective estimate of performance, the ideal information must be known such as target and clutter characteristics. The method is therefore useful in situations where substantial *in situ* information is available, e.g. object positions and other object characteristics. Using information theory, the mutual information of the fused data can be compared to the corresponding information of the separate sources.

Here, information theory will be applied to the spectral imaging of objects and clutter. The amount of mutual information between the source data and the fused data will be studied as a function of dynamic range and the interrelated spectral band selection. The method as used here is requiring detailed masks for both targets and other man-made objects. Other parts of the data will be considered to be genuine clutter. Conclusions from results are therefore only valid with respect to the detailed scenario given. Generalisations have to be made with caution and be based on modelling and simulations.

First, what is meant by spectral information has to be defined. Here, a new approach is being adopted, where the spectral reflectance of an object is characterising the object while the sensor information also is depending on illumination, atmospheric transmission and scattering, spectral responsivity and spatial resolution. In this way, the spectral information of the target varies with the number of pixels on target. The information of spectral clutter varies similarly. Practically, the number of measured spectral features on target varies with

the dynamic range of the measurement and the number of pixels on target. Each spectral feature is considered as being a discrete random variable.

Suppose targets and background clutter occurs randomly in the scene. How much information about what is present in a specific position (features X with values from the set $\{t,b\}$ for target and background) is obtained at a sensor level (features Y with values from the set that is output from the sensor). The conditional probability is $P(Y|X)$. Equivalently, the conditional probability that X is present given the sensor information Y is given by $P(Y|X)$. The quantity of information for events A and B according to Shannon is given by

$$I(A;B) \equiv \log_2 \frac{P(A \mid B)}{P(B)} \tag{20}$$

and the expected value over all outcomes of the stochastic variables X and Y is given by

$$I(X;Y) = \sum_x \sum_y p(x,y) \log_2 \frac{p(x \mid y)}{p(x)} \tag{21}$$

where the unit for I is the "bit."

Observed spectral features, $A=\{y_i\}$, are first obtained for both the known target area ($A_t=\{y_{it}\}$) and the background area ($A_b=\{y_{ib}\}$). Further $A_{tb} = A_t \cap A_b$. There is likely to be common information between A_t and A_b. To the features A, there will be connected a probability for observing that feature in the target area, $P_{i,t}$, and/or in the background area, $P_{i,b}$ where i stands for feature number and t,b stands for target or background. For all $P_{i,t}$ where the corresponding probability $P_{i,b}$ is zero, there will not be any uncertainty whether target or background is present, i.e. $P(A|B)=1$. These features will not contribute to the mutual information since log(1)=0. Only those features that are present both in the target area and in the background area will contribute to the mutual information between target and background. For the present problem,

$$I(\mathrm{X};\mathrm{Y}) = H(\mathrm{X}) - H(\mathrm{X}|\mathrm{Y}) \tag{22}$$

where $H(X)$ is constant and given by

$$H(X) = -\sum_x p(x) \log p(x)\,. \tag{23}$$

and for a binary variable X with probabilities p and 1-p.

$$H(X) = -p \log(p) - (1-p) \log(1-p). \tag{24}$$

The conditional entropy $H(X|Y)$ is now given by

$$H(X \mid Y) = \sum_y p(y) H(X \mid Y = y) \tag{25}$$

and

$$H(X \mid Y = y) = -\sum_x p(x \mid y) \log p(x \mid y) \tag{26}$$

which gives

$$H(X \mid Y) = -\sum_{y \in A_{tb}} p(y) \sum_x p(x \mid y) \log p(x \mid y) \tag{27}$$

where the summation is over non-zero elements, i.e. feature elements common to both the target and the background area.

The mutual information is

$$I(X;Y) = H(X) + \sum_{y \in A_{tb}} p(y) \sum_x p(x \mid y) \log p(x \mid y)\,. \tag{28}$$

The detector is a function which takes observed spectral features as input and determines if the measurement most likely comes from a target or from the background, i. e. each possible observed feature is assigned to the output target or background. For each possible

sensor output the detector has to make a choice whether it believes that the output comes from a measurement on the target or on the background.

The total false alarm probability is given by

$$P_{FA} = \sum_{y \in A_{tb}} p_Y(y) p_{X|Y}(b \mid y) \tag{29}$$

or

$$P_{FA} = \sum_{y \in A_{tb}} p_{Y|X}(y \mid b) p_X(b) \ . \tag{30}$$

$P(A_b|A_t)$=0 means target detection without any false alarms and $P(A_b|A_t)$=1 means an indiscriminate detector with 100 % false alarms. The corresponding target detection probability is given by

$$P_D = \sum_{y \in A_t} p(y) p_{X|Y}(t \mid y) \tag{31}$$

and $P(A_t)$=1 by definition. The optimal receiver operating characteristics (ROC) can be obtained by sorting the relation P_{it}/P_{ib} in descending order and P_{jt} and P_{jb} are now the same probabilities but now sorted in this canonical order. The ROC curve is now obtained by plotting the cumulative detection probability, $P_D(A_{ct})$ against the cumulative false alarm rate $P_{FA}(A_{cb})$ where

$$\begin{aligned} P_D(A_{ct}) &= \sum_{j=1}^{n_c} P_{jt} \\ P_{FA}(A_{cb}) &= \sum_{j=1}^{n_c} P_{jb} \end{aligned} \tag{32/33}$$

and n_c is the number of features above threshold. The ROC curve can be used for estimating optimal sensor performance and to estimate performance gain or loss as a function of sensor parameters.

It is common to normalize the spectrum before running detection algorithms, i.e. $z=x*y$ where x is the normalized spectrum and y is a scalar intensity. This can be done with limited loss of information, provided the spectral shape and spectral intensity are independent and the information in the intensity is very low or $P(z)=P(x)*P(y)$ and $H(P(y))=0$. This might be reasonable for hyperspectral sensors but is becoming less accurate with decreasing number of spectral bands. For a single band, all information is of course in the intensity. A less stringent requirement is that the two probability distributions are independent with the two limiting cases, $P(z)\approx P(x)$ for hyperspectral data and $P(z)\approx P(y)$ for monochromatic data. The advantage using this separation is that objects with similar spectral shape but different intensities can be obtained within the same feature. The intensity contains information on e.g. variations in illumination. Data will however no longer be whitened after normalization. It is not clear that anything is gained from this separation compared to post-processing the results using the original data.

The ROC approach can be used for assessing the variation in performance with respect to variations in the number of spectral bands, the spectral width and extension to other sensors that can be co-registered. Several criteria are in use as a measure of performance. The FAR can be noted at a detection level of a specific percentage of the target. The area under the ROC curve is another measure of the performance. How these measures can be interpreted as a general target detection probability requires further information on target variability and clutter in the specific scene.

7 Preliminary signal processing results

Robust detection of mines and minefields is a challenge. There are many different types of anomaly detection algorithms that can be applied. The performance of the algorithm depends not only on the algorithm itself but also on the detailed feature characteristics of targets and clutter. The algorithms being applied will not be detailed here but the results presented will be indicative to what can be achieved.

The first scenario to be studied is a grass field with a set of mines and man-made clutter situated on the FOI premises. The observed area is 4.8×5.3 m^2 (25 m^2). A false alarm rate of 10^{-3} corresponds to 0.025 m^2 per 25 m^2 area or 0.001 m^2 per 1 m^2.The ground truth is shown in figure 12.

Fig. 12. Targets in the grass area outside the FOI building.

7.1 Hyperspectral sensor in VNIR

Anomaly detection is first shown using the VNIR data. The 17 first detections are presented in fig. 13. Of these objects, two are not identified and two are tentatively identified. Further improvements can be obtained by clustering the anomalies and disregarding clusters associated with the background.

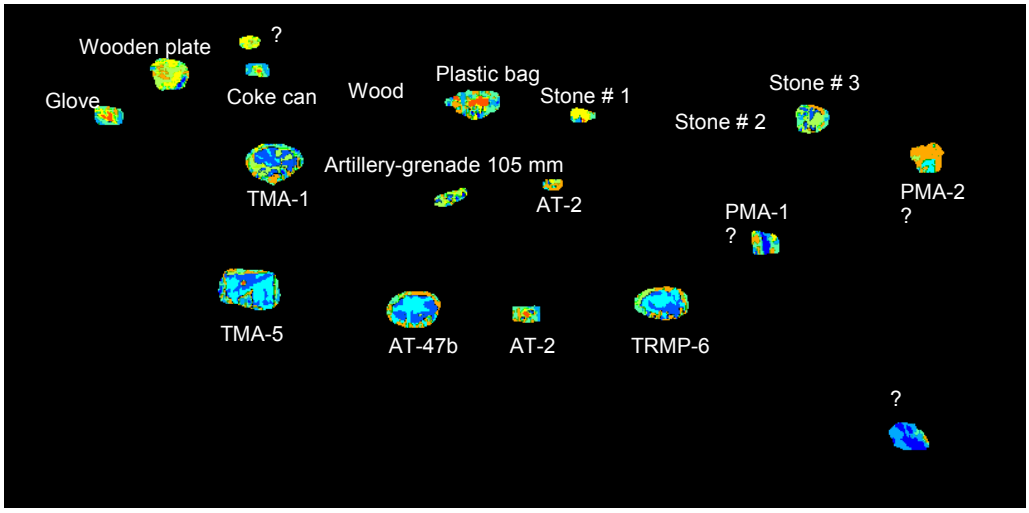

Fig. 13. Results from nearest neighbour anomaly detection using hyperspectral data in the visible and near infrared spectral region. Observed anomalies are subsequently clustered and the result colour coded.

Using only anomaly detections, an estimate of the sensor capability with respect to detecting individual mines can be performed. The detailed ROC curve depends on which objects are being considered as targets and which are considered to be clutter. Here, all man-made objects are masked as targets leaving the variability in the grass field as clutter. This is reasonable since all objects that are not natural in a specific environment must be considered to be an anomaly. The result is also depending on what is the estimated largest object of interest.

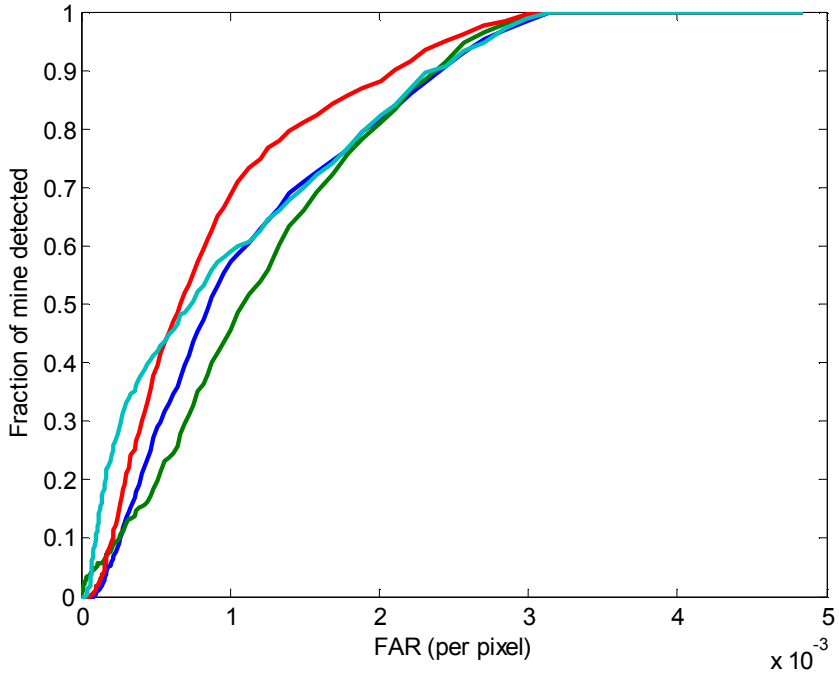

Fig. 14. ROC curves for the four largest mines in the grass field using anomaly detection.

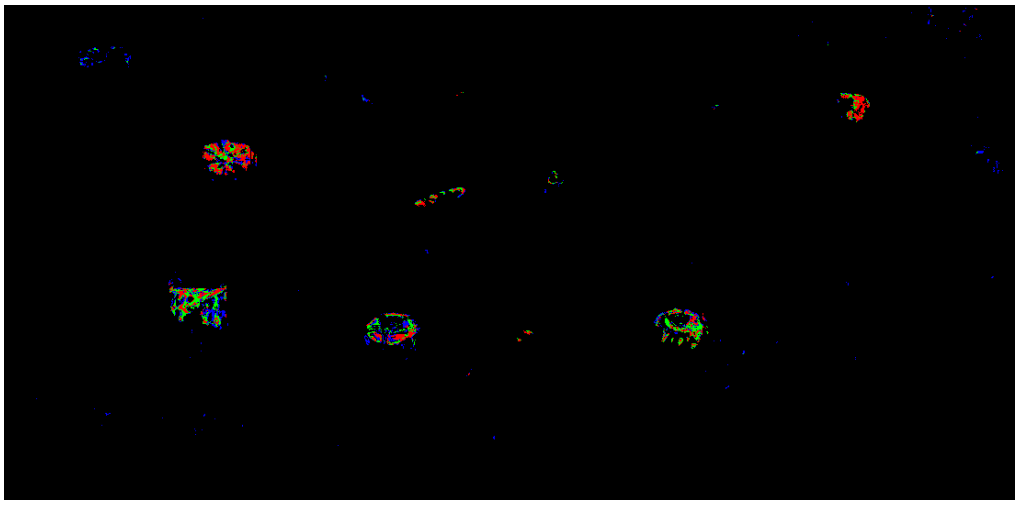

Fig. 15. The spectral content of mine-like objects spectrally similar to TMA-1 are enhanced.

Spectral similarities between objects can be studied by using the spectral features of a known object with a given dynamic range and compare which objects that correlate with this set of features. This gives the optimal separability at this specific dynamic range. An example is given in figure 15 where the spectral properties of TMA-1 are being used. Already at 4 bits of dynamic range, the separability is very good.

In a new test, 25 objects where detected and ordered in decreasing likelihood. The result is shown in figure 16. Knowing in which order the detections are obtained and which ones that corresponds to an identified object, a ROC curve can subsequently be constructed. The ROC curve for this case is shown in figure 17.

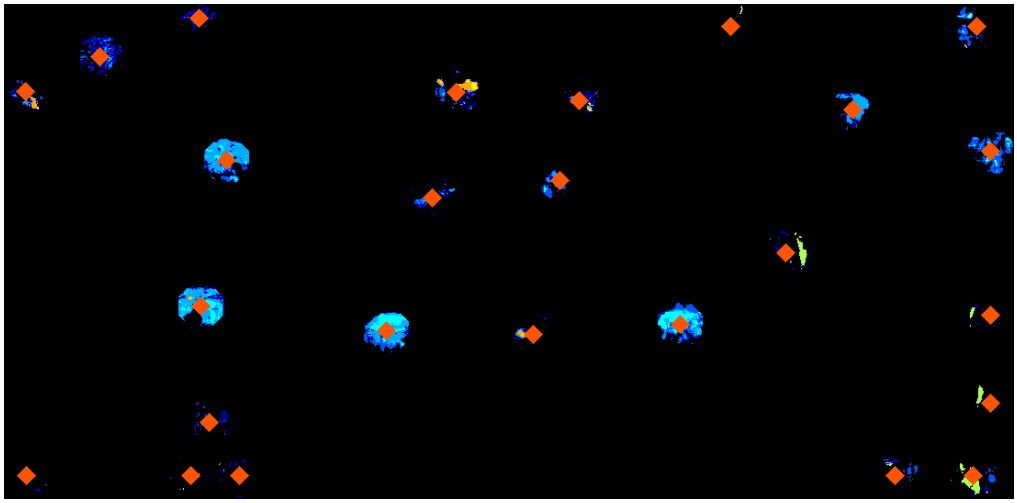

Fig. 16. Detection using nearest neighbourhood detector is shown. Anomalies are clustered but that information is not used in the detection process.

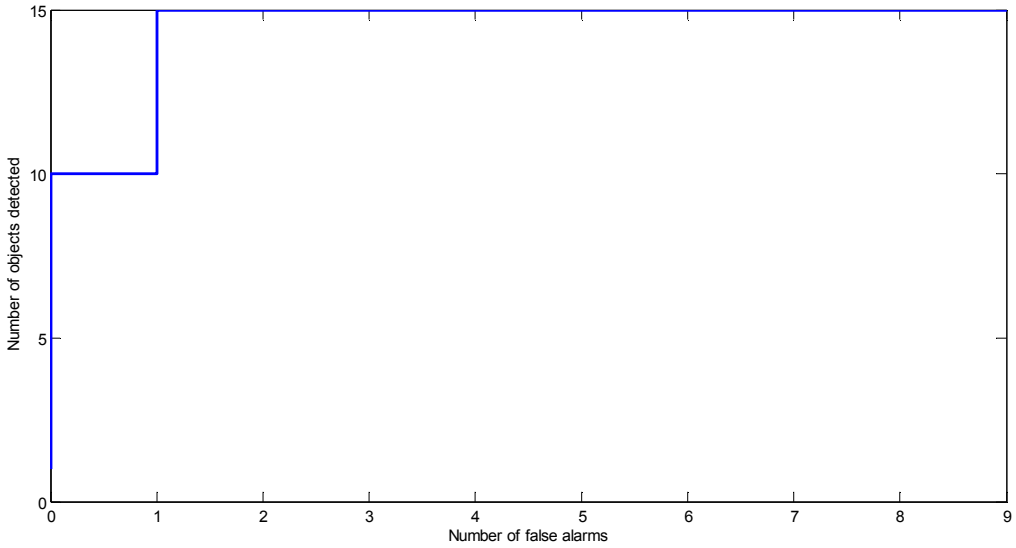

Fig. 17. Very few false alarms are obtained for this case with a simple grass background.

It is interesting to find out how the different targets correlate spectrally. For correlations larger than 0.9, the result for the 25 targets is colour coded and shown in figure 18. Useful results can be obtained even when the dynamic range is reduced to 3 bits, see figure 19. This indicates that spectral information, even when the dynamic range is very low, can contain information useful for discrimination.

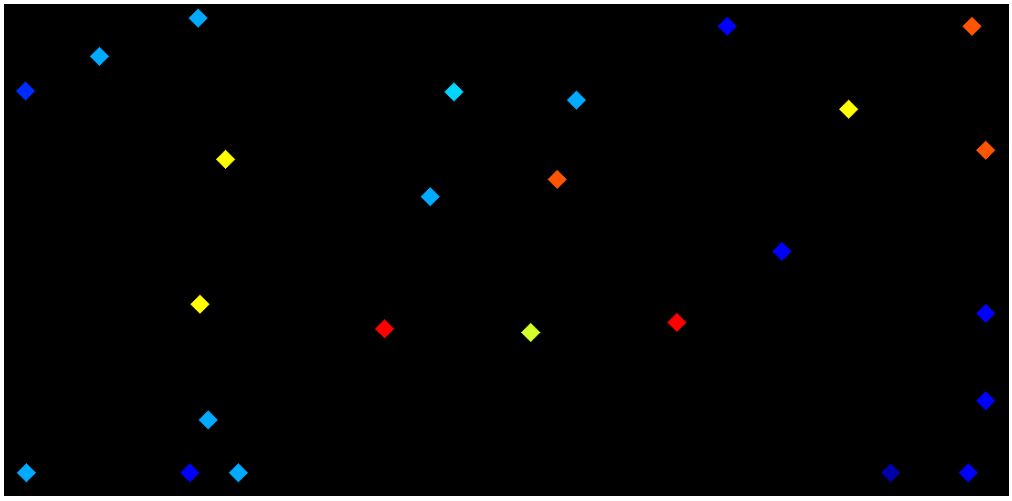

Fig. 18. Correlations between spectral anomalies are shown with 90 % correlation or higher.

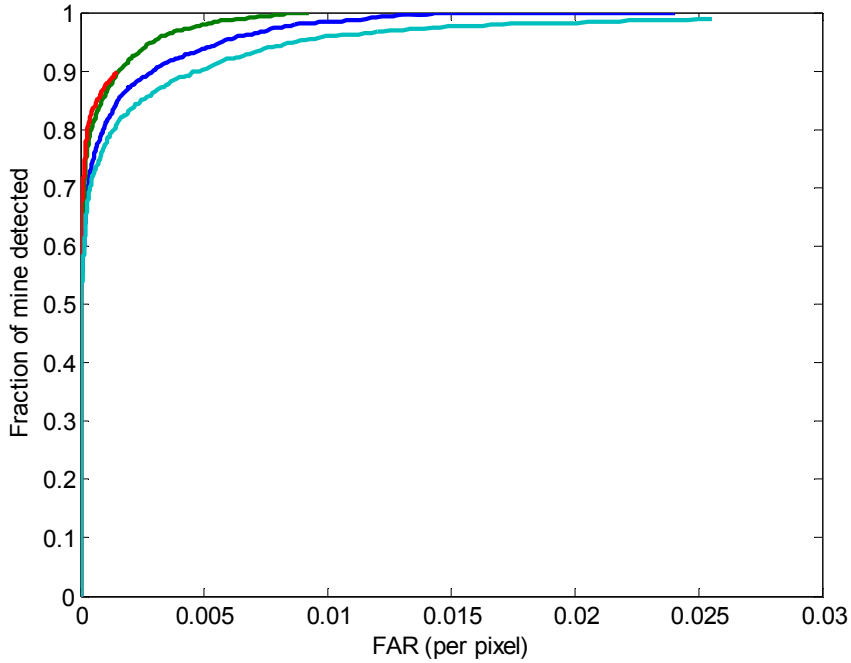

Fig. 19. Detection at 3 bits dynamic range. The targets are the four largest ones, TMA-1, TMA-5, AT-47b and TRMP-6. Note that the FAR scale is different from figure 14.

It might be that reduced scale to a certain extent favours the target to background discrimination capability due to the texture scales. If the background texture contains finer details than for the targets, averaging will reduce the spectral variability in the background faster than the corresponding reduction on target. Increasing the dynamic range to 5 bits and reducing the spatial resolution by binning 4×4 pixels gives the result shown in figure 20. Further reduction in dynamic range results in less useful results.

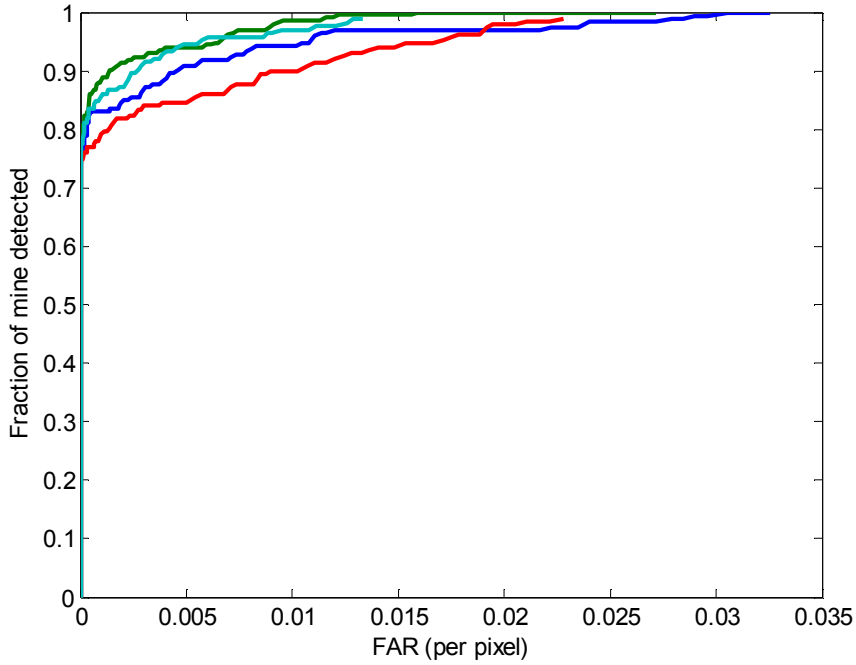

Fig. 20. ROC curve at 5 bits dynamic range and binning by 4×4 pixels. The performance is similar to the previous case with no spatial binning and 3 bits dynamic range.

Even when the scene is compressed by 8×8 blocks, useful results can still be observed. At this reduced scale and at 5 bits dynamic range, the results shown in figure 21 is obtained.

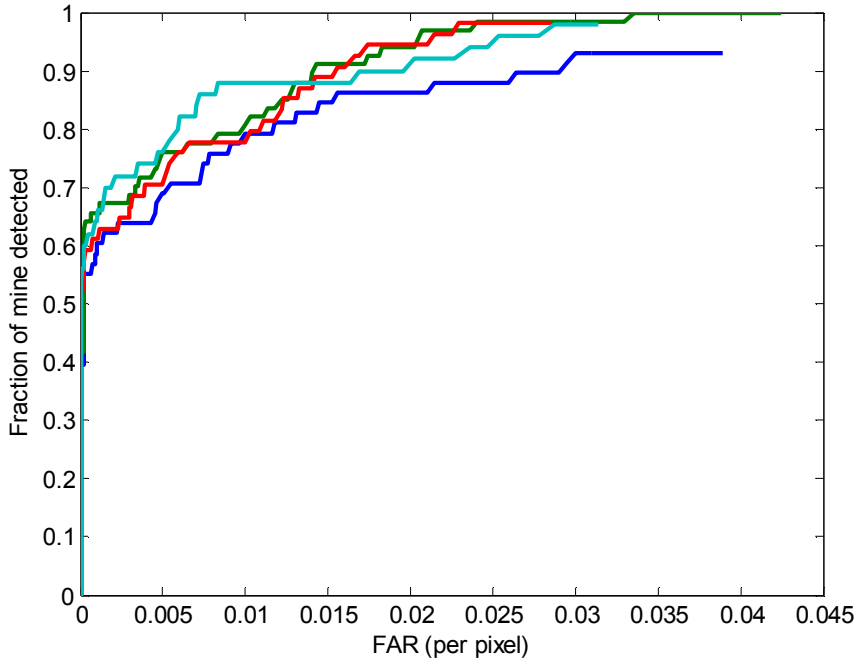

Fig. 21. Reduced performance at 8×8 block averaging and 5 bits dynamic range.

Results when reducing the number of spectral bands is so far inconclusive. This might depend on the larger variability in man-made objects compared to earlier results for camouflaged objects. Further studies are needed in order to find out if multispectral systems with acceptable performance can be designed.

Measurements of mines in backgrounds of varying complexity were performed during the fall under quite unfavourable conditions. The light levels were low with substantial

shadowing. A test of hyperspectral anomaly detection was carried through. The scene is shown in figure 22.

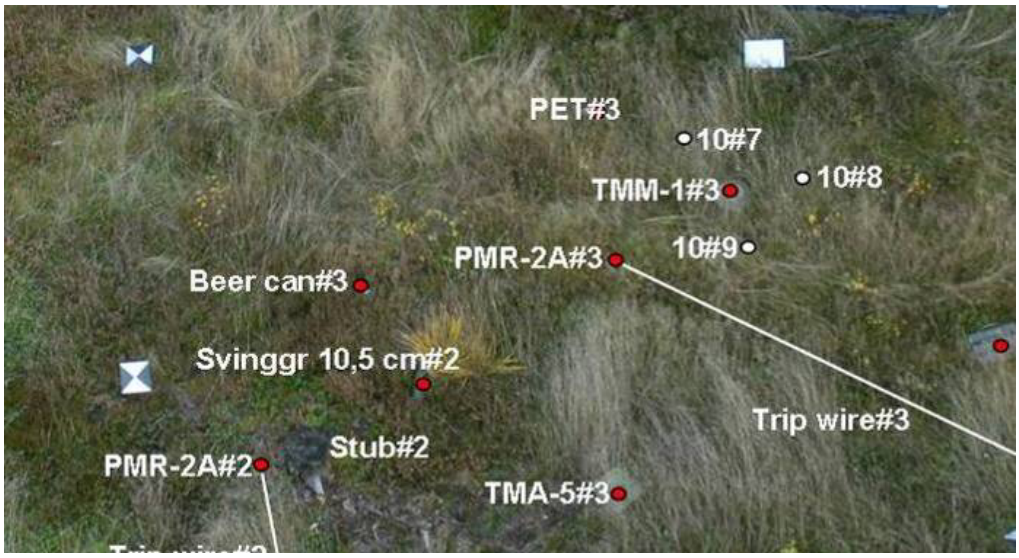

Fig. 22. The grass scene at Eksjö with objects identified in the scene (red points) and other known objects with estimated positions (white points).

The result of the spectral anomaly detector is shown in figure 23 after spectral clustering. The green colour shows object with mine-like characteristics. The results are encouraging also under these very constrained conditions.

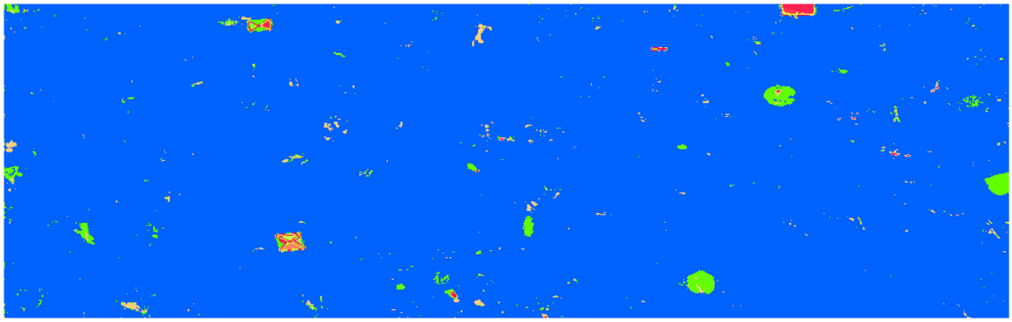

Fig. 23. Anomaly detection and clustering using the scene in figure 22.

Seven of the identified objects were selected for a ROC analysis. Surprisingly good results are obtained, see figure 24. In this situation, active illumination might still further improve on the false alarm reduction.

The ROC curve can generally be further improved by clustering anomalies and invoking a target size dependent detection algorithm. The improvement is shown in figure 25.

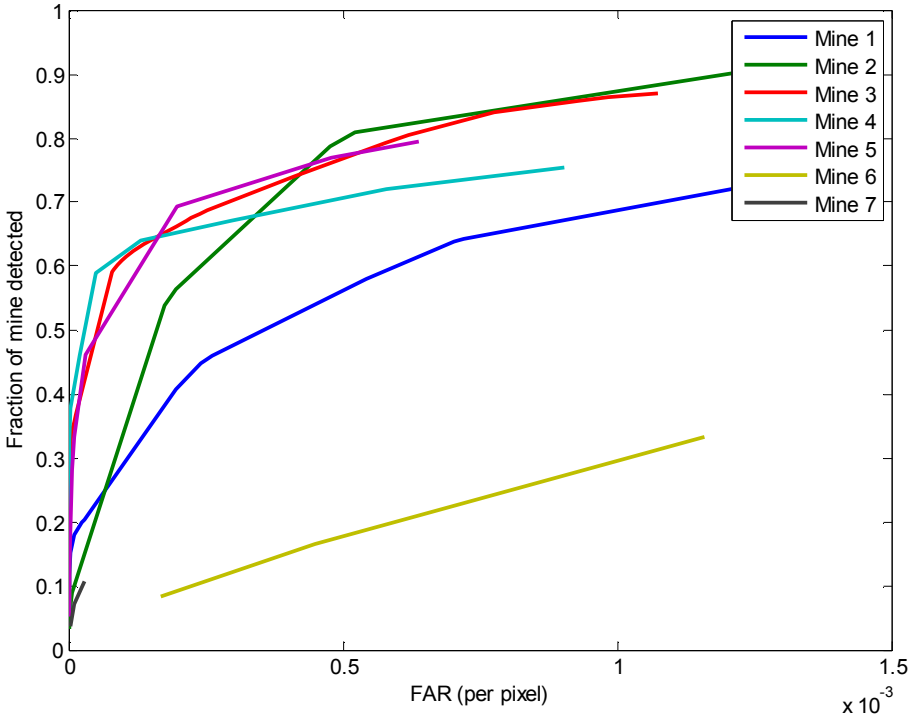

Fig. 24. ROC curves for targets 1 to 7 with 34 bands and 4 bits.

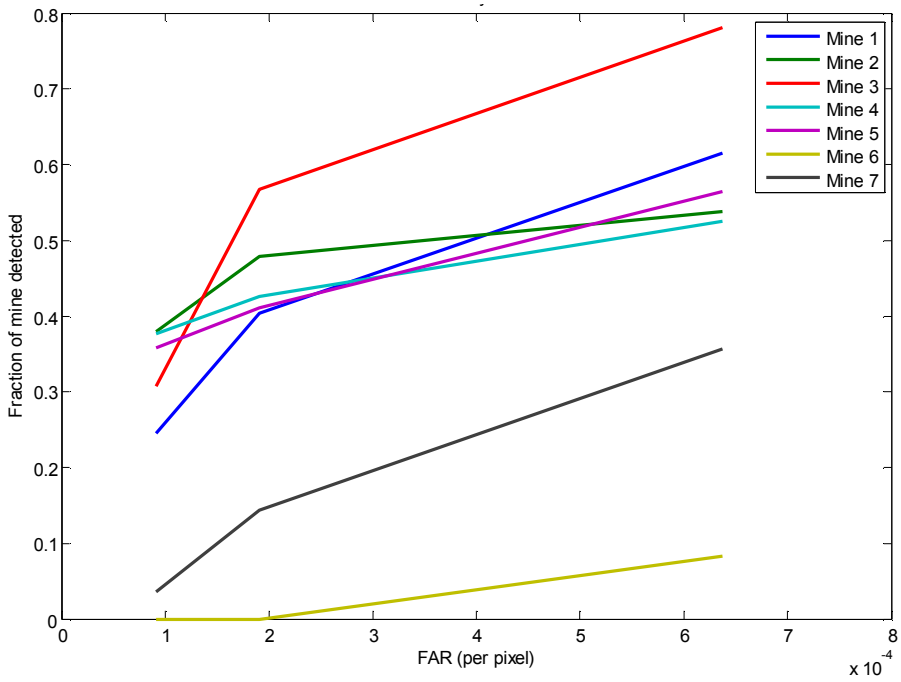

Fig. 25. ROC curves for the same targets as in figure 24 after anomaly clustering.

7.2 Multispectral sensor in SWIR/MWIR

The multispectral camera in the short wave and mid wave infrared spectral region has a rather narrow field of view and high spatial resolution. Anomaly detection is shown using the SWIR/MWIR data from the same mine field as above. First a picture showing mines from parts of the grass area.

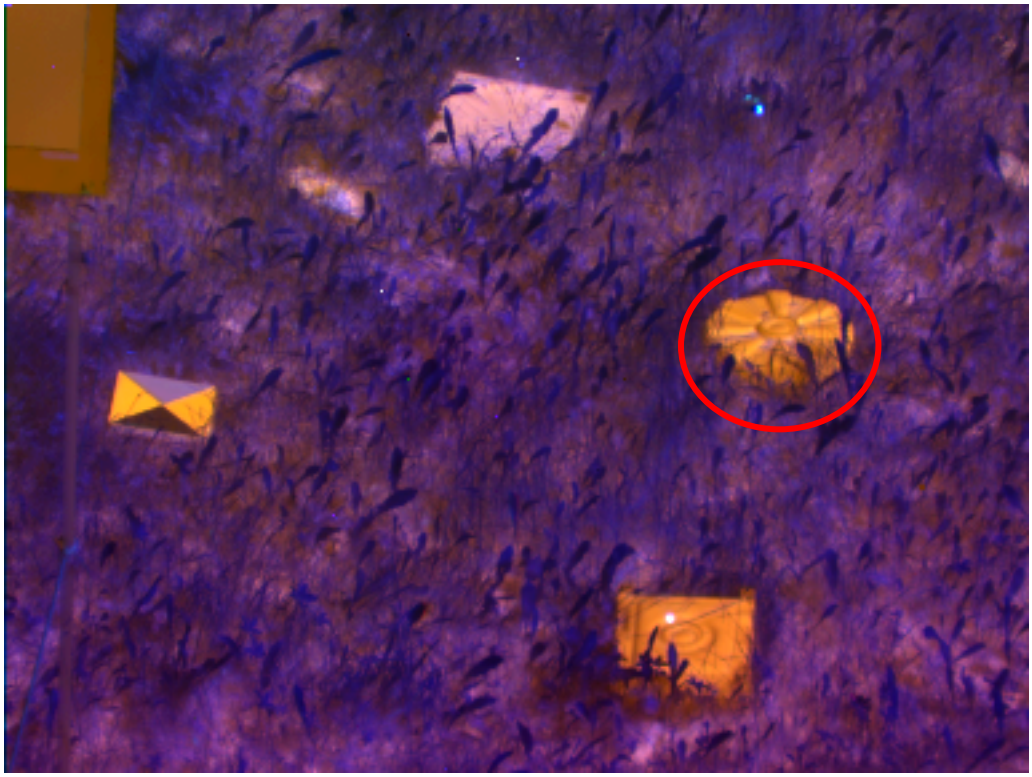

Fig. 26. False colour presentation of parts of the scene using both SWIR and MWIR data.

The anomaly ROC curve is shown in figure 27 for the mine indicated in figure 26. At this spatial resolution, the FAR is very low.

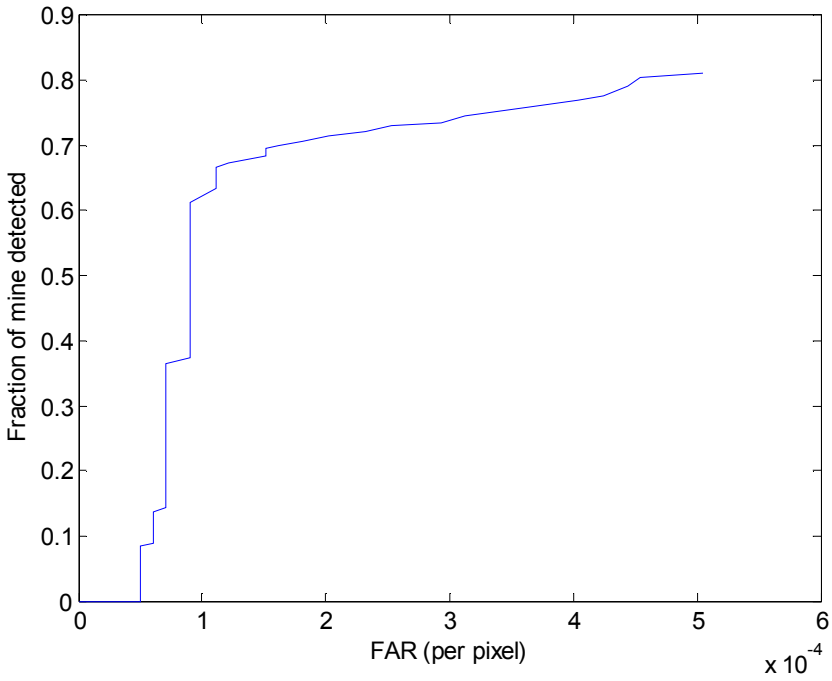

Fig. 27. ROC curve for the mine indicated in the previous figure using full dynamic range anomaly detection.

Clustering the spectral content of the mine under study, using three basis vectors at a dynamic range of 4 bits, results in the target discrimination shown in figure 28. The different colours also indicate which clusters that are present also on interfering objects. The corresponding optimal ROC curve at 4 bits dynamic range is shown in figure 29.

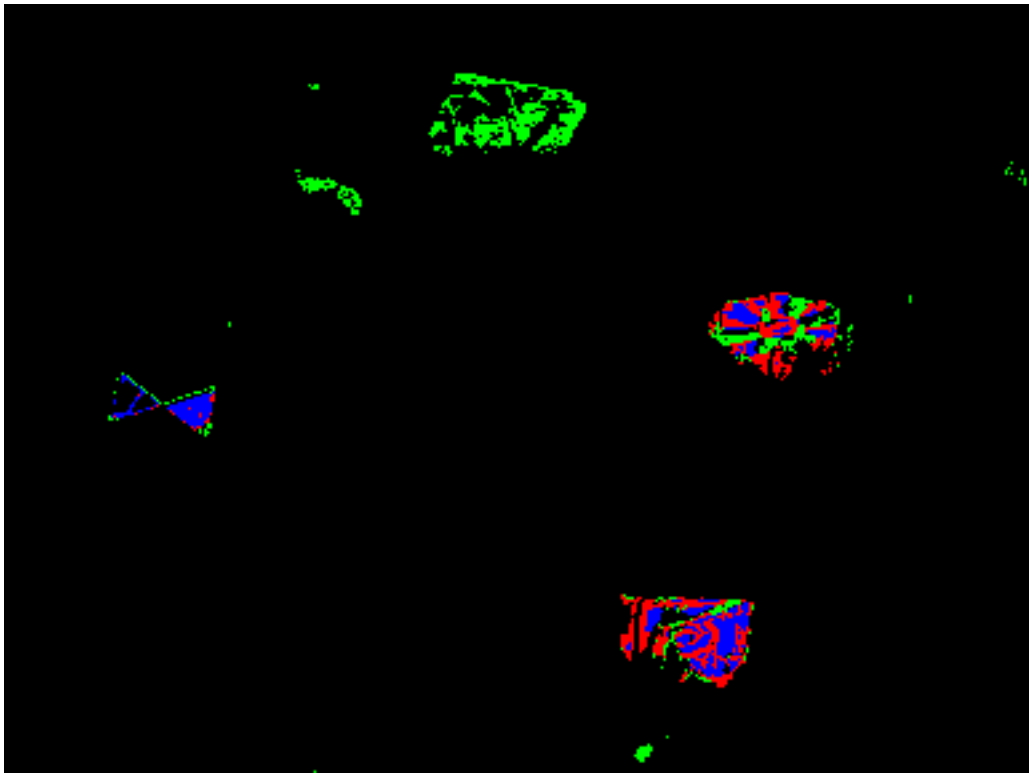

Fig. 28. The three first bases vectors for mine discrimination at 4 bits dynamic range is colour coded.

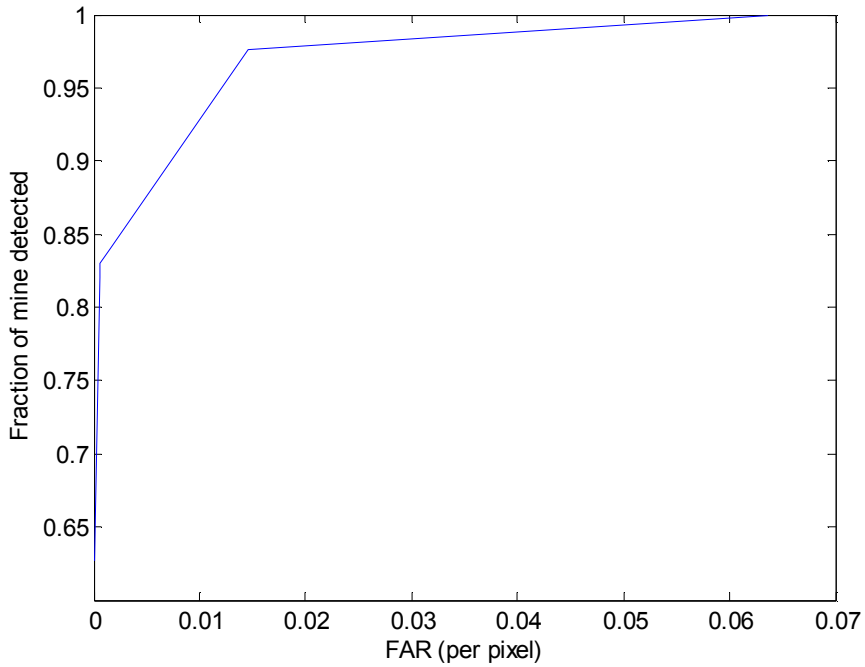

Fig. 29. ROC curve of the multispectral scene shown in figure 26 at a 4 bits dynamic range.

7.3 Long wave thermal infrared sensor

The thermodynamic mechanism of buried objects has previously been extensively modelled [6] and the favourable conditions for detection studied [7]. The thermal behaviour of surface lade objects has been studied in similar ways and the analysis is still progressing. Since the target signature relies on the thermal history, the results are very

weather dependant and detection can therefore not be made on demand. If the thermal history is recorded, improved detection probabilities can be obtained. An example of such a scene sequence is shown below. In figure 30, a sequence of three recordings is colour coded. Differences in colour are a manifestation of differences in thermal history.

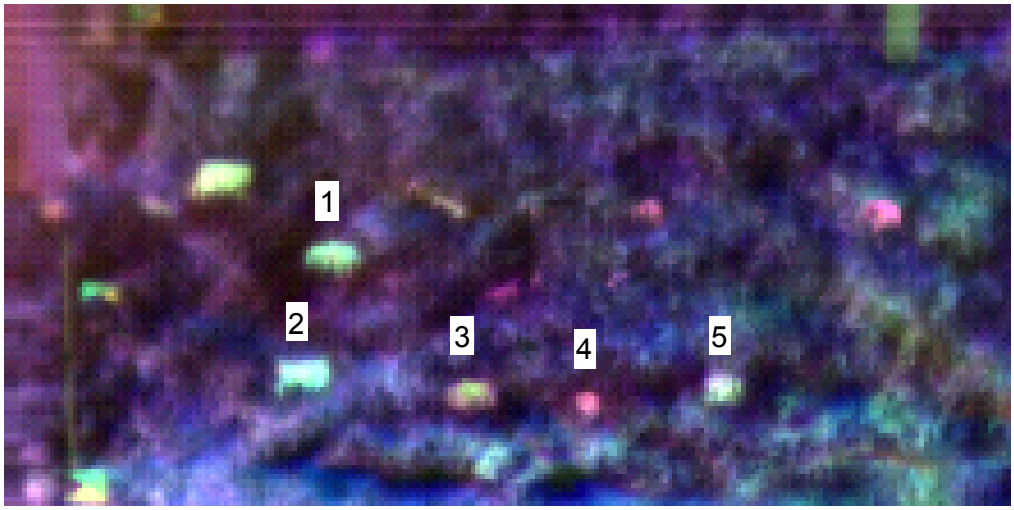

Fig. 30. Three images from three different times are used in order to illustrate the thermal variation. Mines 1 to 5 are discussed below.

The 25 largest anomalies in figure 30 are detected and presented in figure 31. The anomalies are clustered according to the thermal variations and these clusters are also presented in figure 31 using colour coded labels.

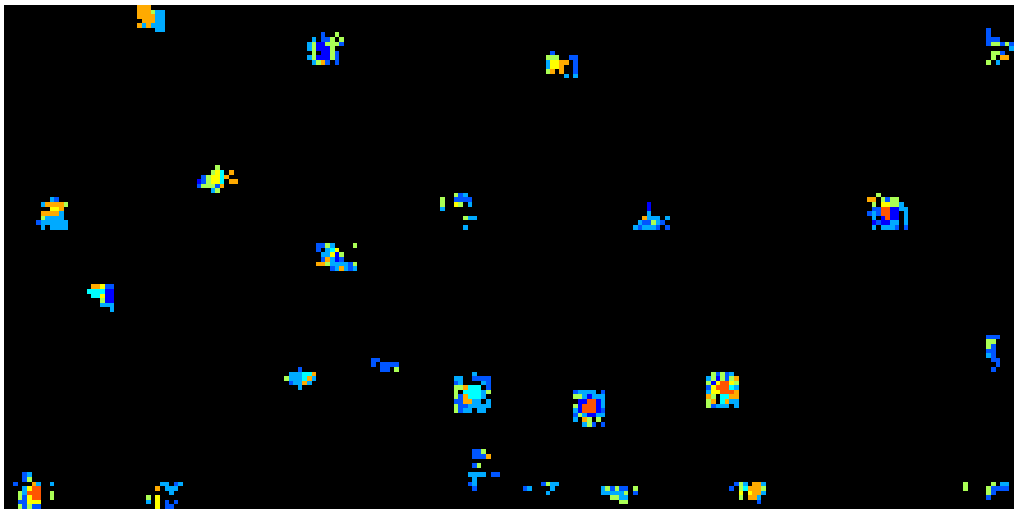

Fig. 31. Detection of 25 objects in the thermal sequence illustrated in figure 30. Detection results has subsequently been clustered.

The objects that can be identified in the scene are designated as targets just as before. The ROC curve for the combined sequence is shown in figure 32.

The number of targets detected in the individual thermal images varies depending on the thermal contrast at that situation. It is therefore expected and also observed that the performance using individual thermal images is lower than for the time sequence. An example is shown in figure 33.

The five targets indicated in figure 30 were also studied for the three separate frames, here called 4, 17 and 34. The fraction of each mine being detected is shown as a function of false alarm rate. It can be seen that frame 17 shows the best performance.

There are many different types of detection algorithms available. Results from a simple Laplace detector is shown in figure 37.

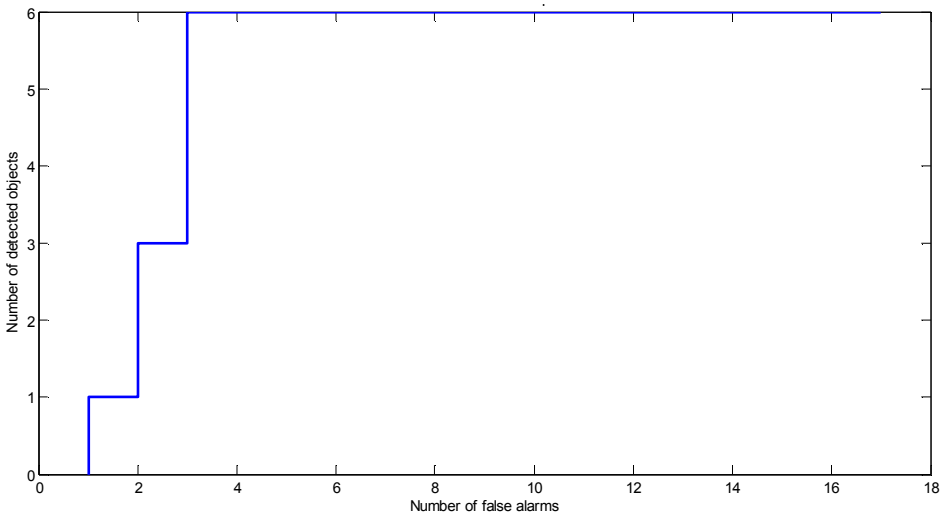

Fig. 32. ROC curve for the thermal time sequence discussed above. The numbered targets are detected with three false alarms.

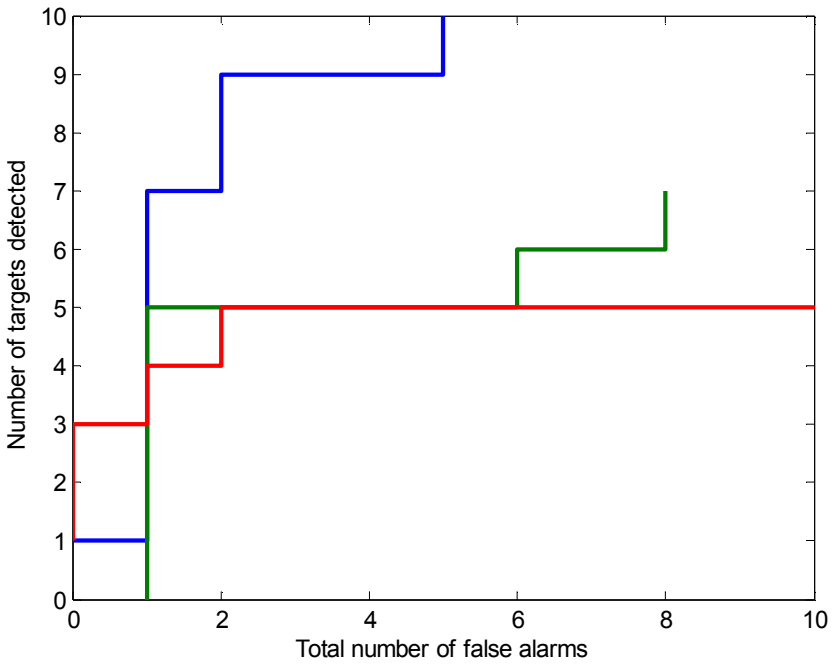

Fig. 33. Total number of targets being detected as a function of total number of false alarms. The result is consistent with the results above.

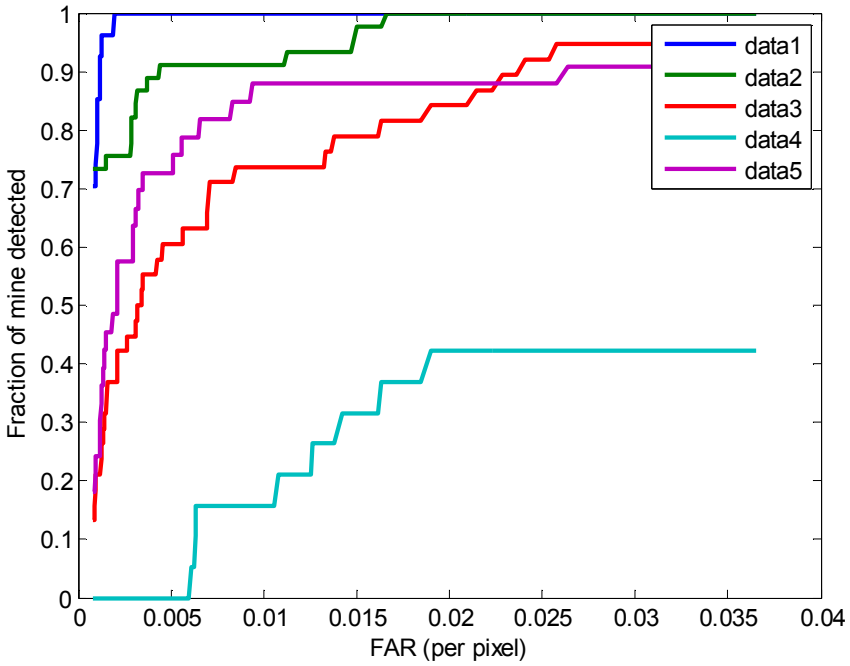

Fig. 34. Illustration of detection capability using frame number 4. Data 1 to 5 refers to mines 1 to 5 as numbered in figure 30.

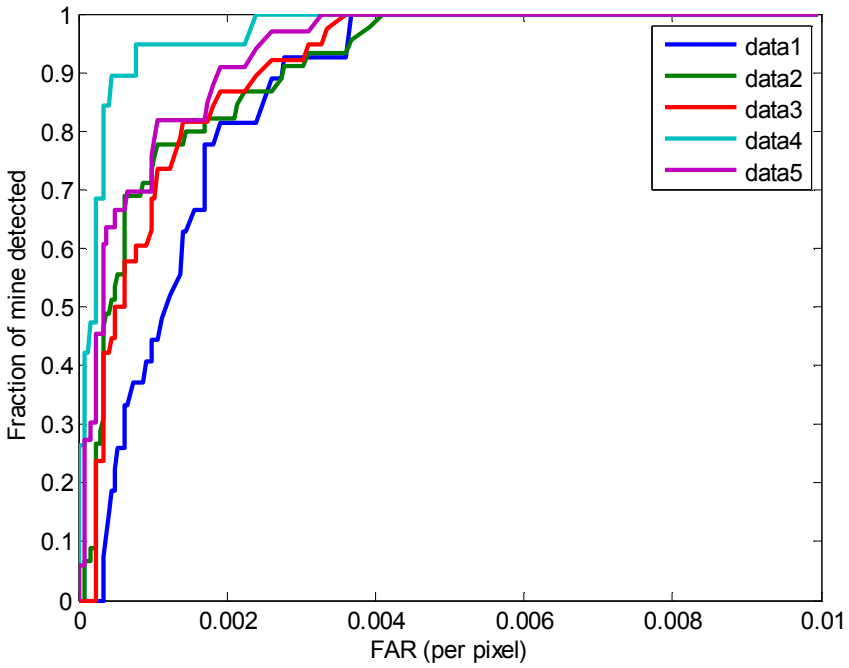

Fig. 35. Illustration of detection capability using frame number 17.

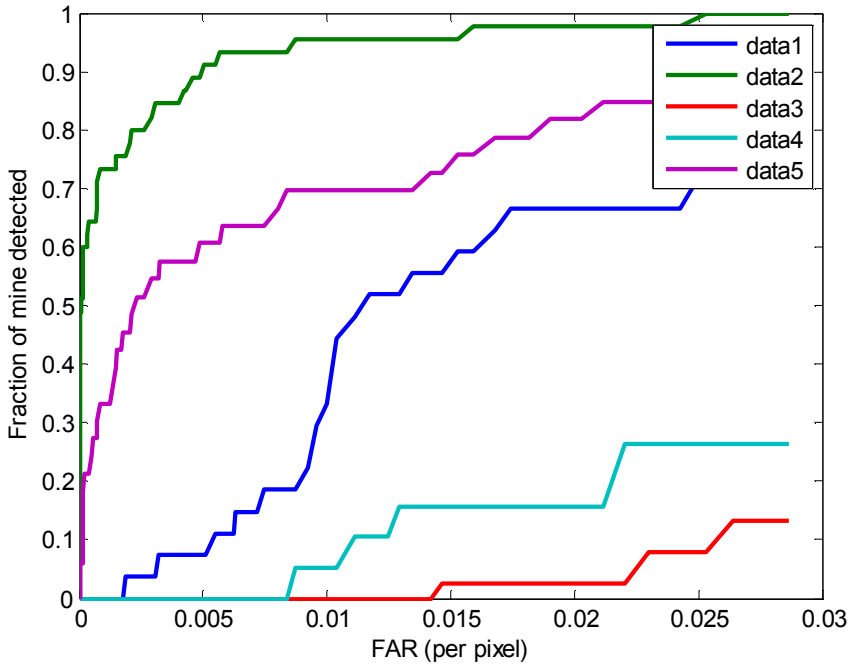

Fig. 36. Illustration of detection capability using frame number 34.

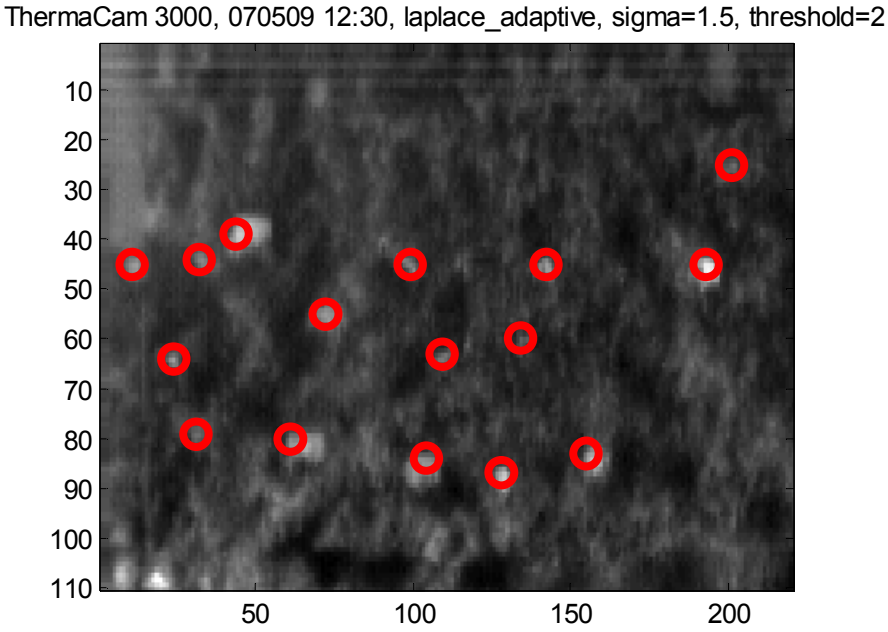

Fig. 37. Detection results using a Laplace detector with σ=1.5.

7.4 White light illumination

Preliminary results from active illumination and multispectral sensing in the visible and near infrared spectral region are quite encouraging. A flashlight was used as an illuminator. The spectral bands of the sensor are not optimized for the purpose and further improvement can therefore be expected. An example of an image showing the grass field with mines at FOI is shown in figure 38.

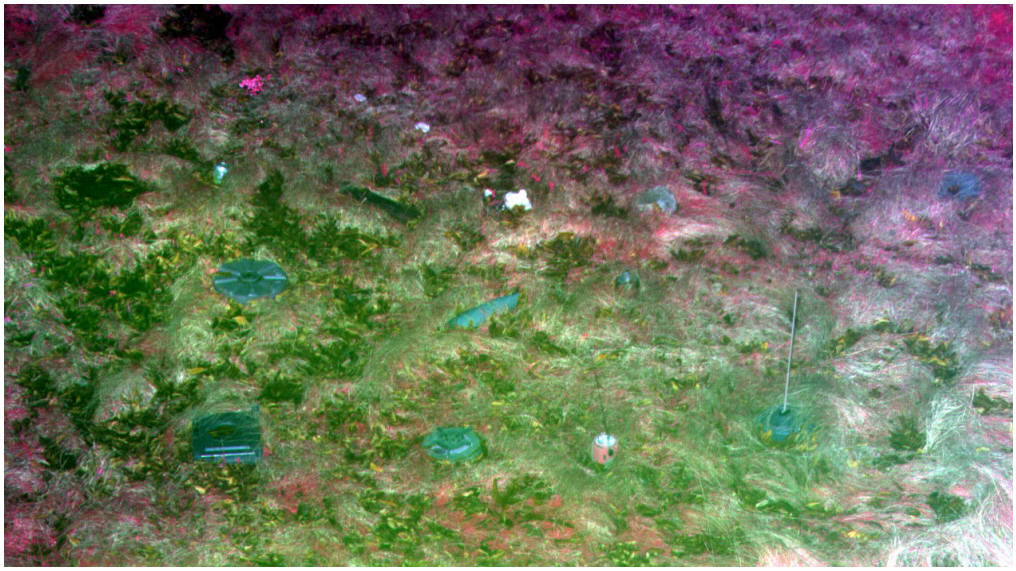

Fig. 38. Multispectral image in the visible and near infrared spectral region.

Nearest neighbour results are shown in figure 39 after clustering. The main objects are detected.

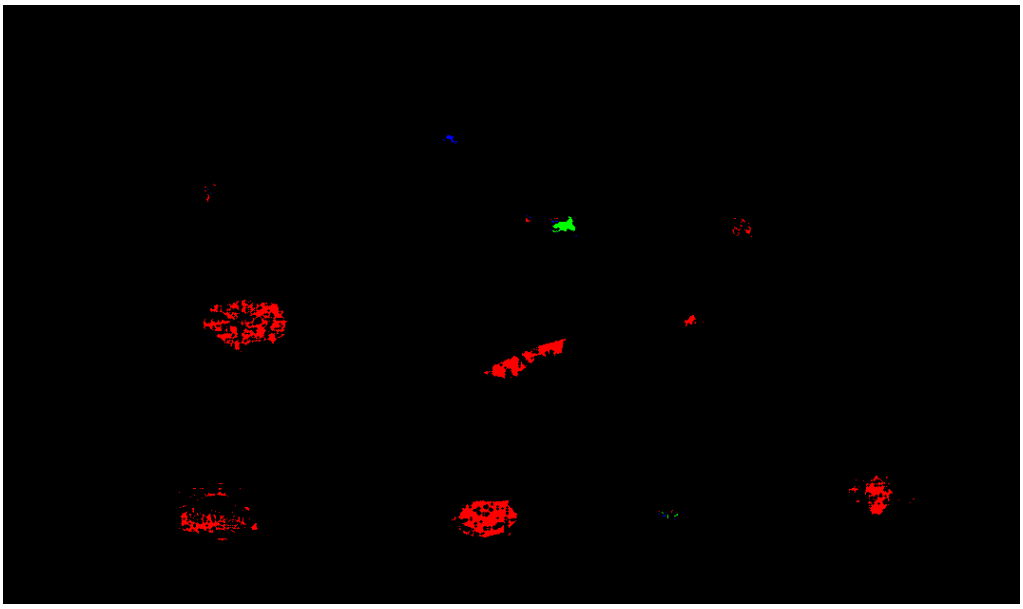

Fig. 39. Anomaly detection after clustering.

A ROC curve with rather high false alarm rate is shown in figure 40. There is, however, information available that could be potentially used for improved performance. This will be further discussed below.

In order to illustrate the potential improvements that can be obtained using alternative processing, an image using PCA analysis is shown in figure 41. This image contains the same information as in image 39. Anomaly detection using component 3 gives the result shown in figure 42.

Results from applying a detection algorithm is shown in figure 43. Only the 25 strongest detections are shown with blue colour indicating strong signal and red indicating weak signal.

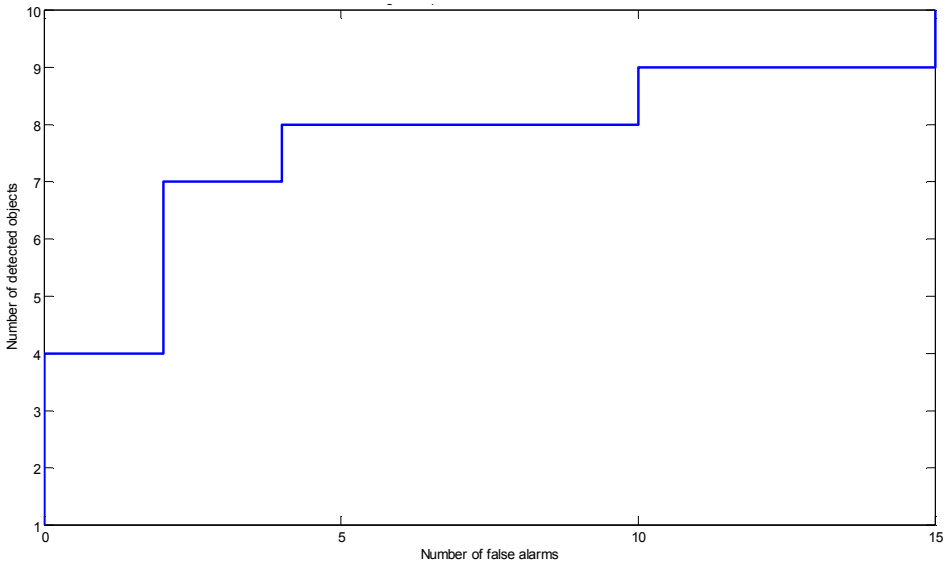

Fig. 40. ROC curve for a multispectral sensor and active illumination.

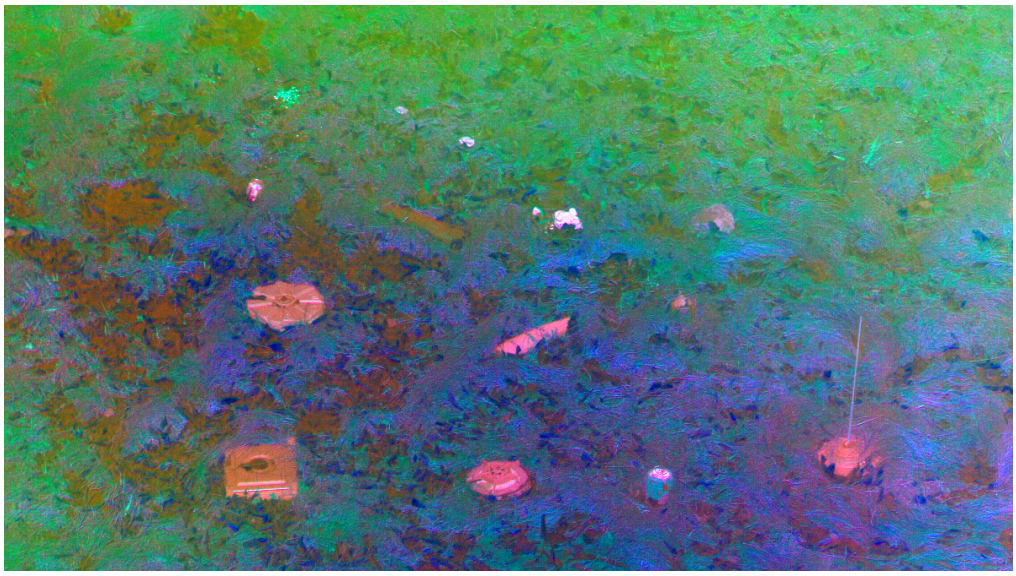

Fig. 41. The image shows the PCA-components 3, 2 and 1 as RGB of the image shown in figure 39.

The same scene was recorded in daylight at a later time. New objects have been added in between, why a direct comparison can not be made. At diffuse illumination, i.e. with a cloudy sky, the performance is quite similar to active illumination. At direct sunlight with sharp shadows, the performance degrades. The daylight scene is shown in figure 44.

Anomaly detection using nearest neighbour is shown in figure 45 after clustering. Performance seems to be better than at active illumination depending on a higher signal level.

Active illumination should be further pursued in order to find out what illumination levels that are needed and what the influence of coherent illumination will be on detection probabilities.

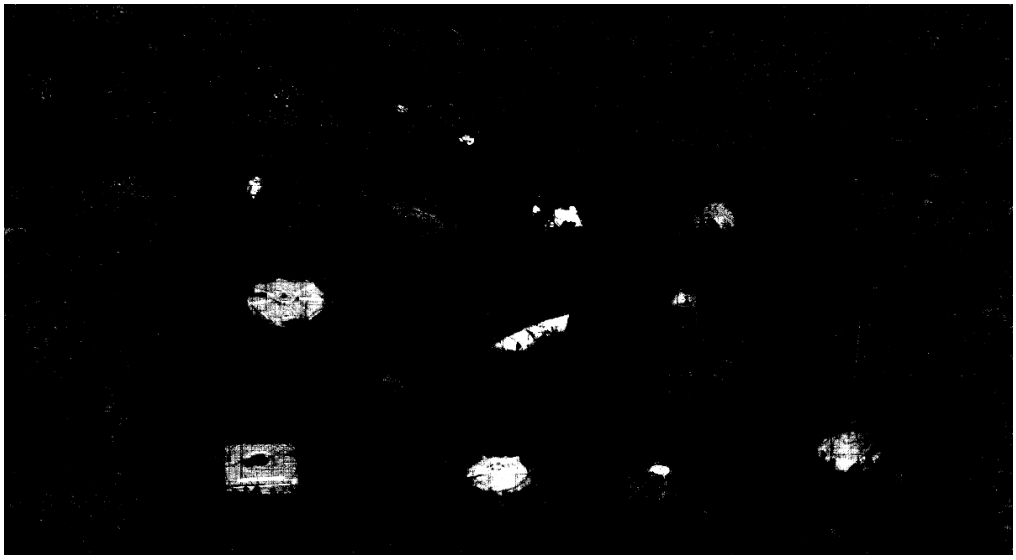

Fig. 42. Detection using the PCA component 3 is exhibiting very low false alarm rate.

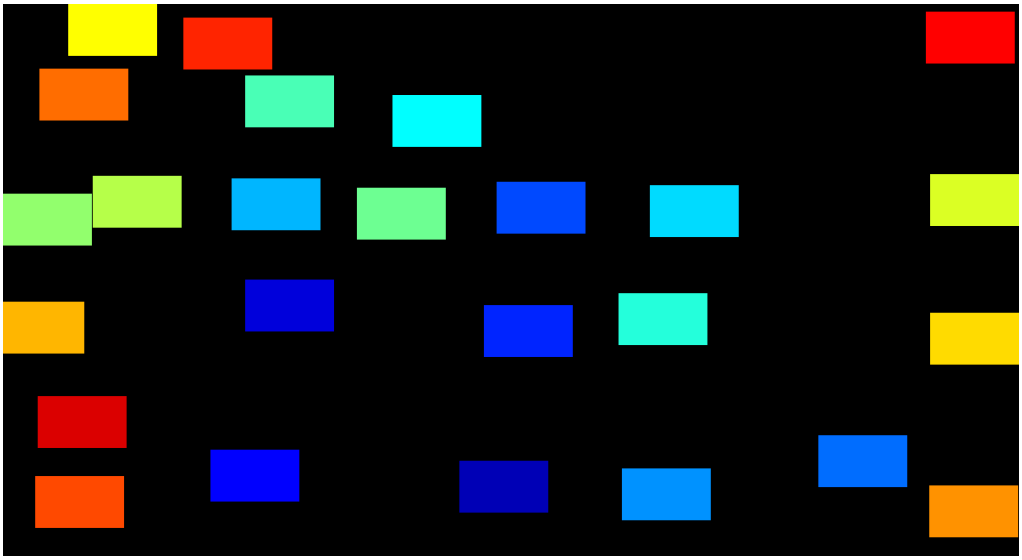

Fig. 43. Detection of 25 targets. Blue targets are detected first and red last.

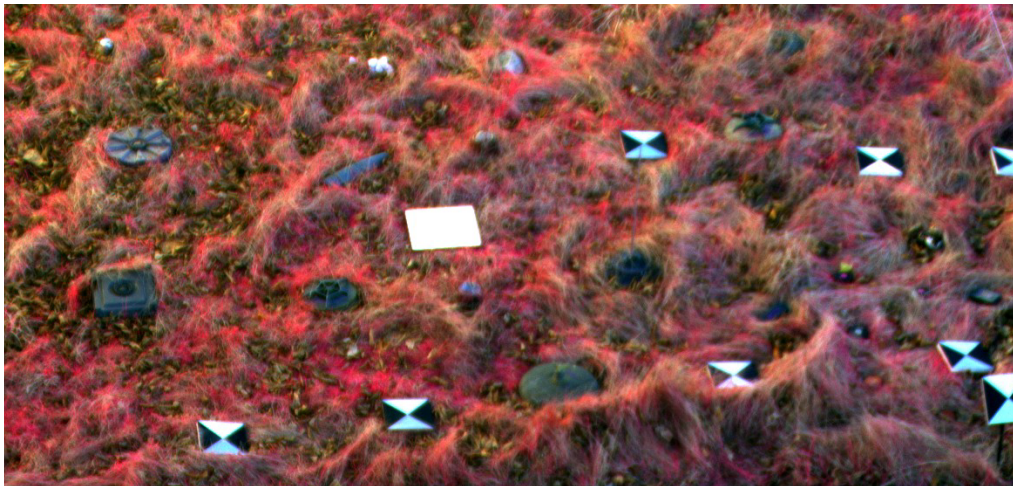

Fig. 44. Daylight scene with clouds using a multispectral camera in the visible and near infrared spectral region.

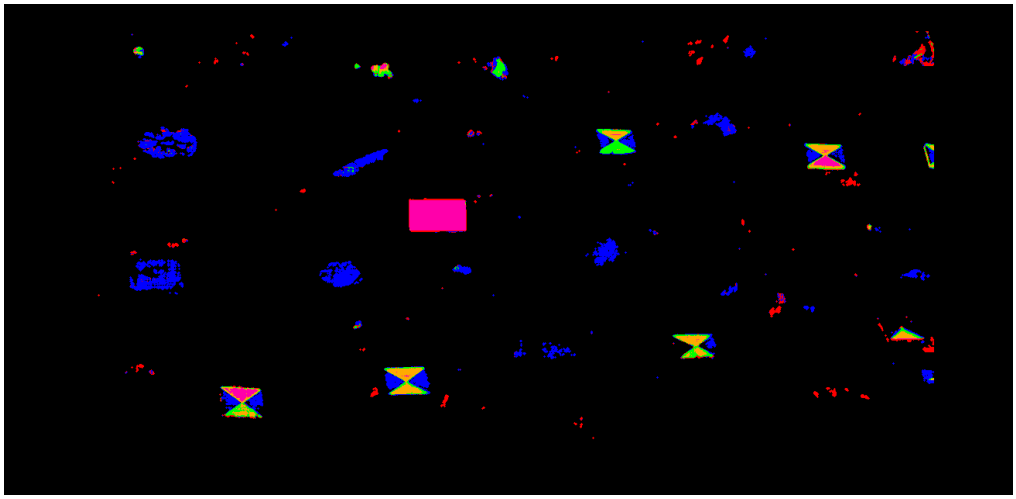

Fig. 45. Anomaly detection using the scene in figure 44.

8 Discussion and conclusions

Hyperspectral imaging has proven to be a powerful technology for object detection and classification. Studies addressing the possibility to reduce the number of spectral channels in order to improve on performance should continue. The trade-off between performance and spatial resolution should also be further studied. This trade-off depends on the spectral variability of the targets versus the corresponding variability of the background clutter. Lower spatial resolution can be translated into larger coverage rate. The present understanding is that relatively high spatial resolution in combination with narrow band widths using hyperspectral imagers are needed for reliable detection. However, multispectral sensors might be possible to design, ones the spectral bands has been carefully selected.

Hyperspectral imaging with day/night capability can be obtained using instrumentation in the thermal infrared spectral region. This technology is not yet well developed in Europe but a number of countries are now vigorously pushing the technology. There is a potential for low cost systems based on un-cooled imaging technology and interferometry. These possibilities should be further pursued.

Sensors relying on the thermal history of objects can not be used on demand. We might have applications when a scene can be monitored over an extended time and where change detection could be of importance. Polarimetric sensing in the thermal infrared region is basically not dependent on the thermal history and can be used for detection. The benefit of this functionality has to be further studied.

Active illumination is of great benefit due to the elimination of shadowing effects. The technologies for both coherent and incoherent illumination should be studied. Another benefit with active illumination is the control of the polarisation state of the illumination that can be exercised. Man made targets and background clutter exhibit very different depolarisation properties and registration of the polarisation state of the backscattered radiation should further improve on the detection and classification capabilities.

Information theory should be applied to the measurements in order to obtain optimal ROC curves that are independent of detection algorithms. The ROC curves that are obtained by applying detection algorithms to the same scene can be compared to these optimal ROC curves. Information theory can also be used for comparing the performance of individual sensors and also for comparison of the mutual information between different sensors. It is important to characterize each individual sensor ahead of combining sensors, sometimes called sensor cueing and sensor fusion.

9 References

1 S. Sjökvist, S. Abrahamson, P. Andersson, T. Chevalier, G. Forssell, C. Grönwall, H. Larsson, D. Letalick A. Linderhed, D. Menning, S. Nyberg, I. Renhorn, M. Severin, O. Steinvall, G. Tolt, and M. Uppsäll, "MOMS Multi Optical Mine Detection System – Initial Report," FOI-R--1721--SE, September 2005.

2 D. Letalick, H. Larsson, A. Linderhed, and I. Renhorn, "MOMS (Multi-optical mine detection system): Progress report 2007," FOI-R--2368--SE, December 2007.

3 J. Ahlberg, "Estimation of atmosphere and object properties in hyperspectral longwave infrared data," FOI-R--2095--SE, October 2006.

4 F. Cremer, W. de Jong, K. Schutte, J. Johnson, and B. Baertlein, "Surface mine signature modeling for passive polarimetric IR," Proc. of SPIE Vol. 4742, *Detection and Remediation Technologies for Mines and Minelike Targets VII*, April, 2002.

5 N. Wadströmer and I. Renhorn, "An information-theoretic model of target discrimination using hyperspectral and multi-sensor data," Proc. of SPIE, Vol. 6940, *Infrared Technology and Applications XXXIV*, to be published.

6 S. Sjökvist, A. Linderhed, S. Nyberg, M. Uppsäll, and D. Loyd, "Land mine detection by IR temporal analysis: Physical numerical modeling," Proc. of SPIE, Vol. 5794, *Detection and remediation technologies for mines and minelike targets X*, pp. 30-41, 2005.

7 A. Linderhed, S. Sjökvist, S. Nyberg, and M. Uppsäll, "Land mine detection by IR temporal analysis: Detection method," Proc. of SPIE, Vol. 5794, *Detection and remediation technologies for mines and minelike targets X*, pp. 21-29, 2005.